Targeting Apoptosis-Inducing Factor as a Novel Therapeutic Strategy for Preventing Perinatal Brain Injury

Juan Rodríguez

Center for Brain Repair and Rehabilitation
Institute of Neuroscience and Physiology
Sahlgrenska Academy, University of Gothenburg

UNIVERSITY OF GOTHENBURG

Gothenburg 2020

Cover illustration: Neuronal mitochondria in a neonatal mouse. The photo was taken at the Centre for Cellular Imaging facility.

Targeting Apoptosis-Inducing Factor as a Novel Therapeutic Strategy for Preventing Perinatal Brain Injury

Juan.rodriguez@gu.se

ISBN 978-91-7833-688-3 (PRINT)
ISBN 978-91-7833-689-0 (PDF)

Printed in Gothenburg, Sweden 2020
Printed by BrandFactory

To my readers,

Targeting Apoptosis-Inducing Factor as a Novel Therapeutic Strategy for Preventing Perinatal Brain Injury

Juan Rodríguez

Center for Brain Repair and Rehabilitation
Institute of Neuroscience and Physiology
Sahlgrenska Academy, University of Gothenburg
Gothenburg, Sweden

ABSTRACT

Perinatal complications such as asphyxia can cause brain injuries that are often associated with subsequent neurological deficits such as cerebral palsy or mental retardation. The mechanisms of perinatal brain injury are not fully understood, but mitochondria play a prominent role, not only due to their central function in metabolism, but also because many proteins with apoptosis-related functions are located in the mitochondrion. Among these proteins, coiled-coil-helix-coiled-coil-helix domain-containing protein 4 (CHCHD4) and apoptosis-inducing factor (AIF) have already been shown to make important contributions to neuronal cell death upon hypoxia-ischemia, but a better understanding of the mechanisms behind these processes is required for the development of improved and more effective treatments during the early stages of perinatal brain injury.

By inducing hypoxia-ischemia in 9-day-old mice, leading to moderate brain injury, we studied these mechanisms from multiple perspectives. The first study of the PhD project was to determine the effect of *chchd4* haploinsufficiency, and we showed that neonatal mice with this genotype experienced less brain damage due to reduced translocation of the apoptosis-related proteins AIF and Cytochrome c from the mitochondrion to the cytosol or nucleus. The second study was to determine the role of a newly discovered AIF isoform (AIF2), which is only expressed in the brain and the functions of which are unknown. By using *Aif2* knockout mice, we showed that under physiological conditions there is an increase in *Aif1* expression (the ubiquitously expressed isoform) due to a compensatory effect of loss of *Aif2* expression. As a result, these mice showed a higher degree of brain damage after hypoxia-ischemia and were more vulnerable to oxidative stress. AIF acts as a free radical scavenger, and from our results it is likely that the AIF2

isoform is more effective serving this task, while AIF1 is a more effective pro-apoptotic protein. The third study used another transgenic mouse in which *Aif* was overexpressed by knocking in a proviral insertion of *Aif*. Our results showed that the insertion increased the expression of *Aif1* without affecting the expression of *Aif2*. This mouse also showed a higher degree of brain damage and higher levels of oxidative stress. Finally, we used a peptide designed to block the apoptotic function of AIF without affecting its pro-survival role. The results in young mice showed that the neuroprotective effect of the peptide was greater in male mice than in female mice.

In conclusion, this PhD project has opened new perspectives in the comprehension of the mechanisms by which CHCHD4 and AIF are crucial proteins for brain damage after hypoxia-ischemia, and it has showed that AIF is a promising therapeutic target for improving outcome after perinatal brain injury.

Keywords: AIF, AIF/CypA complex, apoptosis, asphyxia, CHCHD4, hypoxia-ischemia, mouse, neonatal

ISBN 978-91-7833-688-3 (PRINT)
ISBN 978-91-7833-689-0 (PDF)

SAMMANFATTNING PÅ SVENSKA

Perinatala komplikationer såsom syrebrist kan orsaka hjärnskador som ofta är förknippade med efterföljande neurologiska konsekvenser såsom cerebral pares eller intellektuella funktionsnedsättningar. Mekanismerna bakom perinatal hjärnskada är inte fullt klarlagda, men mitokondrier spelar en framträdande roll, inte bara på grund av deras centrala roll i ämnesomsättningen, utan även för att många proteiner med apoptosrelaterade funktioner finns i mitokondrierna. Bland dessa proteiner har coiled-coil-helix-coiled-coil-helix domain-containing protein 4 (CHCHD4) och apoptosis-inducing factor (AIF) redan visats bidra till neuronal celldöd vid hypoxi-ischemi (syrebrist), men en större förståelse för mekanismerna bakom dessa processer krävs för utveckling av bättre och effektivare behandlingar under de tidiga stadierna av perinatal hjärnskada.

Genom att inducera hypoxi-ischemi i nio dagar gamla möss, vilket leder till måttlig hjärnskada, studerade vi dessa mekanismer ur flera perspektiv. Doktorandstudiens första projekt var att bestämma effekten av *chchd4*-haploinsufficiens, och vi visade att neonatala möss med denna genotyp fick minskade hjärnskador tack vare minskad translokation av de apoptosrelaterade proteinerna AIF och Cytokrom c från mitokondrierna till cytosolen eller cellkärnan. Den andra studien var att bestämma rollen för en nyupptäckt AIF-isoform (AIF2), som bara uttrycks i hjärnan och vars funktioner är okända. Genom att använda *Aif2*-knockout-möss visade vi att det under fysiologiska förhållanden finns en ökning av *Aif1*-uttrycket (den allmänt uttryckta isoformen) på grund av en kompensatorisk effekt för förlusten av *Aif2*-uttrycket. Som ett resultat uppvisade dessa möss en högre grad av hjärnskada efter hypoxi-ischemi och var mer sårbara för oxidativ stress. AIF oskadliggör fria radikaler, och våra resultat tyder på att AIF2-isoformen gör detta mer effektivt medan AIF1 är framförallt ett pro-apoptotiskt protein. Den tredje studien använde en annan transgen mus där *Aif* var överuttryckt. Våra resultat visade att *Aif* knock in ökade uttrycket av *Aif1* utan att påverka uttrycket av *Aif2*. Denna mus visade också en högre grad av hjärnskada och högre nivåer av oxidativ stress. Slutligen använde vi en peptid utformad för att blockera den apoptotiska funktionen hos AIF utan att påverka dess överlevnads funktioner. Resultaten hos unga möss visade att peptidens hjärnskyddande effekt var större hos hanmöss än hos honmöss.

Sammanfattningsvis visade detta doktorandprojekt att CHCHD4 och AIF är viktiga proteiner vid hjärnskada efter hypoxi-ischemi och att de är lovande terapeutiska mål för att förbättra utfallet efter perinatal hjärnskada.

RESUMEN EN ESPAÑOL

Complicaciones perinatales como la asfixia pueden causar lesiones cerebrales que están asociados con déficits neurológicos posteriores, como son la parálisis cerebral o la discapacidad intelectual. Los mecanismos de la lesión cerebral perinatal no se conocen en su totalidad, pero las mitocondrias juegan un papel fundamental, no solo por su rol central en el metabolismo, sino también porque muchas proteínas relacionadas con la apoptosis se encuentran en la mitocondria. Entre estas proteínas, CHCHD4 y AIF han demostrado su importancia en la muerte celular neuronal tras la hipoxia-isquemia (HI). Sin embargo, se requiere una mayor comprensión de los mecanismos detrás de estos procesos para el desarrollo de mejor y más efectivos tratamientos durante las primeras etapas de la lesión cerebral perinatal.

Al inducir HI en ratones de 9 días de edad, provocando una lesión cerebral moderada, estudiamos estos mecanismos desde múltiples perspectivas. El primer estudio de este proyecto de doctorado fue determinar el efecto de la haploinsuficiencia del gen *chchd4*, y demostramos que estos ratones experimentaron un menor daño cerebral, debido a una reducción en la translocación mitocondrial de las proteínas apoptóticas AIF y Citocromo c. El segundo estudio trató sobre determinar el papel de una isoforma de AIF recientemente descubierta (AIF2), que solo se expresa en el cerebro y cuyas funciones son desconocidas. Mediante el uso de ratones *Aif2*-knockout, mostramos que, en condiciones fisiológicas, hay un aumento en la expresión de *Aif1* (la isoforma expresada ubicuamente) debido a un efecto compensatorio, consecuencia de la pérdida de *Aif2*. Como resultado, estos ratones mostraron un mayor grado de daño cerebral después de la HI y fueron más vulnerables al estrés oxidativo. AIF desempeña una función asociada a eliminar radicales libres, y de nuestros resultados se deduce que la isoforma AIF2 sería más efectiva para esta tarea, mientras que AIF1 estaría más relacionada con la función pro-apoptótica. El tercer estudio utilizó un ratón transgénico en el que *Aif* se sobreexpresó usando una inserción proviral que provocó un aumento de la expresión de *Aif1* sin afectar a *Aif2*. Este ratón transgénico también mostró un mayor grado de daño cerebral y mayores niveles de estrés oxidativo. Finalmente, en un cuarto estudio utilizamos un péptido diseñado para bloquear la función apoptótica de AIF sin afectar su papel pro-supervivencia. Los resultados mostraron que el efecto neuroprotector del péptido fue mayor en ratones macho que en ratones hembra.

En conclusión, este proyecto muestra que CHCHD4 y AIF son proteínas cruciales para el daño cerebral post-HI y que AIF es una diana terapéutica prometedora para el tratamiento del daño cerebral perinatal.

LIST OF PAPERS

This thesis is based on the following studies, referred to in the text by their Roman numerals.

I. Sun Y, Li T, Xie C, Xu Y, Zhou K, Rodriguez J, Han W, Wang X, Kroemer G, Modjtahedi N, Blomgren K, Zhu C. "Haploinsufficiency in the mitochondrial protein CHCHD4 reduces brain injury in a mouse model of neonatal hypoxia-ischemia."
Cell Death & Disease 8, no. 5 (2017): e2781.

II. Rodriguez J, Zhang Y, Li T, Xie C, Sun Y, Xu Y, Zhou K, Huo K, Wang Y, Wang X, Andersson D, Ståhlberg A, Xing Q, Mallard C, Hagberg H, Modjtahedi N, Kroemer G, Blomgren K, Zhu C. "Lack of the brain-specific isoform of apoptosis-inducing factor aggravates cerebral damage in a model of neonatal hypoxia–ischemia."
Cell Death & Disease 10, no. 1 (2018): 3.

III. Li T, Li K, Zhang S, Wang Y, Xu Y, Cronin S, Sun Y, Zhang Y, Xie C, Rodriguez J, Zhou K, Hagberg H, Mallard C, Wang X, Penninger J, Kroemer G, Blomgren K, Zhu C. "Overexpression of apoptosis inducing factor aggravates hypoxic-ischemic brain injury in neonatal mice."
Submitted to *Cell Death & Disease*.

IV. Rodriguez J, Xie C, Li T, Sun Y, Xu Y, Li K, Wang Y, Zhou K, Mallard C, Hagberg H, Doti N, Wang X, Zhu C. "Inhibiting the interaction between apoptosis inducing factor and cyclophilin A prevents brain injury in neonatal mice after hypoxia-ischemia."
Submitted to *Neuropharmacology*.

CONTENTS

ABBREVIATIONS

3-NT	3-nitrotyrosine
8-OHG	8-hydroxyguanosine
AAs	Amino acids
AIF	Apoptosis-inducing factor
ATP	Adenosine triphosphate
BCL-2	B-cell lymphoma 2
BLBP	Brain lipid-binding protein
bp	Base pairs
BrdU	5-bromo-2-deoxyuridine
CA1	Cornu ammonis 1
Caspase	Cysteine-aspartic proteases
CHCHD4	Coiled-coil-helix-coiled-coil-helix domain-containing protein 4
CL	Contralateral
COX1	Cytochrome c oxidase subunit I
CP	Cerebral palsy
CypA	Cyclophilin A
Cyt c	Cytochrome c
DCX	Doublecortin
DG	Dentate gyrus
DRP1	Dynamin-1-like protein
Epo	Erythropoietin
FAD	Flavin adenine dinucleotide
FIS1	Mitochondrial fission 1
GSH	Glutathione
H2AX	H2A histone family member X
HI	Hypoxia-ischemia or hypoxic-ischemic
HIE	Hypoxic-ischemic encephalopathy
Hq	Harlequin
HSP70	Heat shock protein 70
IL	Ipsilateral
IMM	Inner mitochondrial membrane
kDa	Kilodaltons
KO	Knock-out

KEGG	Kyoto encyclopedia of genes and genomes
KI	Knock-in
MAP2	Microtubule-associated protein 2
MBP	Myelin basic protein
MDA	Malondialdehyde
Mff	Mitochondrial fission factor
MFN	Mitofusion
MIMS	Mitochondrial intermembrane space
MLS	Mitochondrial localization sequence
MOMP	Mitochondrial outer membrane permeabilization
MPP	Mitochondrial-processing peptidase
NAD	Nicotinamide adenine dinucleotide
NeuN	Neuronal nuclei
NH	Nucleus habenularis
NLS	Nuclear localization sequences
NO	Nitric oxide
OPA1	Optic atrophy 1
OxPhos	Oxidative phosphorylation
PAR	Poly-ADP ribose
PARP-1	Poly (ADP–ribose) polymerase 1
PBS	Phosphate-buffered saline
PCR	Polymerase chain reaction
PGC1α	Peroxisome proliferator-activated receptor γ coactivator-1α
PGK	Phosphoglycerate kinase promoter
PUMA	p53-upregulated modulator of apoptosis
ROS	Reactive oxygen species
RT-qPCR	Quantitative reverse transcription PCR
SGZ	Subgranular zone
Smac	Second mitochondria-derived activator of caspases
SOD2	Superoxide dismutase 2
TAT	Trans-activator of transcription
TFAM	Mitochondrial transcription factor A
TH	Therapeutic hypothermia
TMD	Transmembrane domain
Veh	Vehicle
WT	Wild type

1 INTRODUCTION

1.1 HYPOXIC-ISCHEMIC ENCEPHALOPATHY

Hypoxic-ischemic encephalopathy (HIE) is a condition that is associated with oxygen deprivation in the neonate due to perinatal asphyxia. Despite important progress in neonatal care over the last decades, HIE is still an important contributor to neonatal mortality and to major neurodevelopmental disabilities, including mental retardation, cerebral palsy (CP), learning disabilities, and seizures [1; 2; 3]. Due to improvements in perinatal care and the increased survival rate of infants born with a low gestational age, the absolute number of subjects affected by these complications has increased. The incidence of HIE ranges from 1 to 8 per 1,000 live births in developed countries, but underdeveloped countries have reported incidences of up to 26 per 1,000 live births [4; 5; 6; 7; 8]. Perinatal brain injury can occur in newborns at any gestational age, but preterm and very preterm babies (meaning that the baby was born alive with less than 37 or less than 32 weeks of pregnancy, respectively) are less prepared to adapt to perinatal insults compared to term infants, making them more vulnerable to neurodevelopmental impairments due to hypoxia-ischemia (HI) [9; 10]. Although premature babies are able to tolerate more prolonged periods of hypoxia - ischemia, the effect can dramatically alter the normal development in the immature brain [11; 12]. HIE can be ranked in three clinical stages according to the widely accepted Sarnat scoring system as mild, moderate, and severe encephalopathy [13]. The few infants who survive severe HIE will most likely develop life-long complications [14], while for moderate HIE some estimations made in Sweden on a small group of individuals born in the 1980s suggest that about 30–40% of the survivors develop CP or other major neurological impairments, and another 30–40% develop cognitive problems [15]. Other studies showed that untreated moderate to severe HIE results in an approximately 60% risk of either death or major neurological impairments [16; 17; 18].

Nowadays, the most common treatment for infants with HIE is based on therapeutic hypothermia (TH) applied during the first 6–10 hours after HI [6; 19]. This treatment has shown that HI injury can be mitigated by reducing the risk to approximately 50% [17]. The current standard of TH in neonates with moderate to severe HIE is based on whole-body cooling (or just head cooling, but the temperature inside the brain does not decrease as much as with whole-body cooling) to a core temperature of 33.5ºC for 3 days [20]. It is very important that this treatment starts within 6–10 hours after birth [21], during

the latent phase between the primary and secondary energy failure [22], as suggested by several studies in which TH applied during the latent phase has been associated with an optimal long-lasting neuroprotection [23; 24].

TH has led to great improvements in neurocognitive outcomes and reduced mortality [25]. The reason behind TH's treatment efficiency is the reduction in cerebral metabolism along with reduced excitotoxic neurotransmitter accumulation, reduced adenosine-triphosphate (ATP) depletion, and reduced oxygen and nitrogen free radical release [26]. However, TH is not a suitable treatment for preterm infants because it has been shown to be risky for them [27]. TH has also failed as a therapeutic strategy for severely affected children [28]. Furthermore, TH does not provide full neuroprotection, and about 40%–50% of neonates with moderate to severe HIE still suffer severe neurological complications or die after TH [17].

One option suggested to improve the outcome of HIE patients is to use TH together with other pharmacological adjuvants to increase neuroprotection and/or to promote neural regeneration. In this respect, low doses of recombinant human erythropoietin (Epo) hormone have shown positive effects in the long-term outcome for infants with moderate (but not severe) HIE [26; 29], and with only minor side effects observed [30]. Epo has been shown to have anti-inflammatory, anti-excitotoxic, anti-oxidative, and anti-apoptotic properties [31; 32]. Apart from TH and Epo, other substances have been proposed for improving HIE outcome [33], including melatonin, which has anti-apoptotic, anti-inflammatory, and antioxidant properties [34; 35]. Xenon, allopurinol, and magnesium sulfate have also been found to be promising for HIE treatment, but further studies are needed [36; 37].

1.2 MOLECULAR MECHANISMS OF HIE

HIE in newborn infants causes brain injury that lasts for several days due to mechanisms of cellular apoptosis, autophagy, necrosis, and inflammation, and mitochondria play extremely important roles in these processes [38; 39; 40]. The type of cell death depends on several factors, including the severity of the insult, the cell type, the metabolic stress, the sex of the infant, and the elapsed time since the event [38]. This evolving process can be divided into two main phases.

1.2.1 THE PRIMARY PHASE

The primary phase starts immediately after the insult. HI induces a reduction in the cerebral blood flow leading to a depletion of the oxygen and glucose

supply to the brain. This results in impairment of ATP formation due to the disruption of ATP-dependent processes, such as failure of the Na/K pump that leads to depolarization of the cell membrane [40]. As a consequence, the cell releases the excitatory amino acid glutamate into the extracellular space, which cannot be reabsorbed by adjacent neurons and glia because these mechanisms are ATP-dependent, thus leading to an accumulation of glutamate to excitotoxic levels and the over-activation of N-methyl-D-aspartate receptors, which increases the intracellular Ca^{2+} level [39]. This is followed by mitochondrial dysfunction and the generation of reactive oxygen species (ROS) and nitric oxide (NO), which will induce mitochondrial outer membrane permeabilization (MOMP) and the subsequent release of proapoptotic proteins from the mitochondrial intermembrane space (MIMS) to the cytosol [41], as will be discussed later in more detail. These changes imply a shift in cellular metabolism from oxidative to anaerobic glycolysis metabolism with an increase in the intracellular levels of inorganic phosphate, lactate, and hydrogen ions, thus producing lactic acid and leading to intra- and extracellular acidosis.

1.2.2 THE SECONDARY PHASE

If the insult is a transitory episode, the restoration of cerebral blood flow will lead to normalization of mitochondrial function, intracellular pH, energy metabolism, and oxygen concentration. However, a secondary mitochondrial energy failure can occur within about 6–15 hours after the first insult. The reasons behind this secondary deterioration are still unknown, but this phase will lead again to an increase in intracellular levels of Ca^{2+}, unregulated release of excitatory amino acids such as glutamate, further mitochondrial dysfunction and generation of ROS and NO, and the release of proapoptotic proteins and inflammatory molecules [42; 43; 44; 45; 46].

This biphasic pattern of injurious mechanisms gives us a therapeutic window in which neuroprotective strategies can be considered in order to rescue brain cells that are damaged but still not committed to cell death (if considering autophagy, ferroptosis or paraptosis as forms of cell death), and thus improve the outcome of the infant's life after the episode of HI.

1.3 APOPTOSIS

Two main apoptotic pathways occur in the cell – the extrinsic pathway mediated by death receptors, and the intrinsic pathway mediated by the mitochondria [38; 41]. Both routes take place through multiple molecular mechanisms and are related to each other, such that the molecular events of

one influence the other. Contrary to the extrinsic pathway (which is triggered by extracellular signals that oligomerize death receptors located on the plasma membrane [47]), the intrinsic pathway is triggered by intracellular stimuli such as an increase of ROS, NO, and Ca^{2+} caused by glutamate overflow. This will cause mitochondrial impairment and the increased expression of the pro-apoptotic B-cell lymphoma 2 (BCL-2) protein family [48]. Subsequently, MOMP will occur causing the release from the mitochondria to the cytosol of pro-apoptotic proteins such as cytochrome c (Cyt c), apoptosis-inducing factor (AIF), second mitochondria-derived activator of caspases (Smac), and endonuclease G [38], making this a crucial event for another way to classify apoptosis, depending on the final executor, and that differ in their dependence or independence on cysteine-aspartic proteases (caspases). Caspase-dependent apoptosis is initiated by Cyt c and the assembly of the apoptosome leading to the activation of caspase 3 [49], which will cut the DNA into small pieces of about 200 to 1000 base pairs (bp) [50]. The caspase-independent pathway (also known as "parthanatos") terminates with the translocation of AIF to the nucleus where it will cause large-scale DNA fragmentation (into pieces of about 50,000 bp) and chromatin condensation [41].

Under physiological conditions, AIF is a vital protein for obtaining energy in the mitochondria (among other functions), but upon apoptotic stimuli AIF will undergo a change and become pro-apoptotic. This switch from a pro-survival to a pro-apoptototic protein is controlled by different mechanisms.

The first mechanism involves MOMP, which is regulated by several proteins and serves as a good example of how the caspase-dependent and caspase-independent pathways are related to each other – the extrinsic pathway activates caspase 8, which in turn can activate the protein BID (a BCL-2 family member protein, also known as BH3 interacting-domain death agonist). The BID protein, together with other members of the BCL-2 family proteins such as BCL-2-associated X protein (BAX) and BCL-2 homologous antagonist killer 1 (BAK1), will be activated, and this is a crucial step for MOMP and pore formation [51] and the consequent release of cell death related proteins that belong to both, caspase-dependent and caspase-independent pathways. Second, AIF is regulated by the activation of calpain and cathepsin proteases, which are needed to cleave AIF from the inner mitochondrial membrane (IMM) [52; 53]. Third, AIF's apoptotic function is controlled by the heat shock protein 70 (HSP70) chaperone, which can neutralize AIF by binding to the specific HSP70-binding domain located in amino acids (AAs) 150–228 of the mature AIF [54]. Lastly, AIF is also regulated by poly (ADP–ribose) polymerase 1 (PARP-1), which is a nuclear enzyme involved in DNA repair by producing poly-ADP ribose (PAR) polymers using nicotinamide-adenine

dinucleotide (NAD^+). However, in case of excessive DNA damage caused by severe genomic stress (such as that resulting from HI), overactivation of PARP-1 can drain the cellular NAD^+ supply and cause energy depletion [55]. PARP-1 has been suggested to be a key contributor to cell death, and indeed the term parthanatos is being used now to refer to the caspase-independent apoptotic pathway based on the over activation of PARP-1 and the consequent NAD^+ depletion [56]. In addition, PARP-1 overactivation participates in the translocation of AIF from the mitochondria to the nucleus, and in a *PARP-1* knock out (KO) study in mice, neurons fail to release AIF to the nucleus in response to apoptotic stimulus [57].

Apoptosis is a crucial process in the immature brain [58], and it determines the appropriate development of the central nervous system. Unsurprisingly, many components of the intrinsic pathway, as well as proteins involved in apoptosis (such as caspase 3, BCL-2 family proteins, and AIF) are upregulated during brain development [38]. Indeed, these apoptotic mechanisms, including nuclear translocation of AIF, Cyt c release, and caspase 3 activation, have been found to be more prominent in immature than in juvenile and adult mouse brains [59].

1.4 APOPTOSIS-INDUCING FACTOR

AIF (full gene name: Apoptosis-inducing factor, mitochondria-associated 1; *AIFM1*) is a flavin adenine dinucleotide (FAD)-dependent, NAD^+ oxidoreductase that, under physiological conditions, is located in the MIMS [60]. The most abundant transcript, called *AIFM1* (Gene ID: 26926 in mice; Gene ID: 9131 in humans), possesses a transcribed region encoded in 16 exons that generates a 67 kilo Dalton (kDa) precursor molecule of 613 AAs in humans (612 AAs in mice). AIF1 has three domains: an FAD-bipartite binding domain (AAs 129–262 and AAs 401–480), an NADH-binding motif (AAs 263–400), and a C-terminal domain (AAs 481–608) [61]. In addition, there are two mitochondrial localization sequences (MLSs) placed one after the other in the N-terminal region (AAs 1–41) and two nuclear localization sequences (NLS1 and NLS2) located within the two FAD-binding domains [62]. The MLS drives the transportation of AIF into the MIMS [63; 64]. Once there, AIF will undergo the first proteolytic cleavage and thus be processed to a mature form (62 kDa) (Figure 1). AIF is then inserted through its amino-terminal transmembrane segment into the IMM, leaving the rest of the protein exposed to the MIMS [65].

The amino-terminal transmembrane domain (TMD) encompasses AAs 54 (where the mitochondrial-processing peptidase (MPP) cleavage site is located)

to 103 (where the calpain/cathepsin cleavage site is located). Within the amino-terminal transmembrane segment is the transmembrane domain (AAs 67–83). AIF also has two binding domains: one for HSP70 at AAs 150–228 (included in the FAD-binding domain) and the other for cyclophilin A (CypA) at AAs 367–399 and included in the NADH-binding motif. AIF also possesses two DNA-binding sites located in AAs 255–265 and 510–518 (Figure 1).

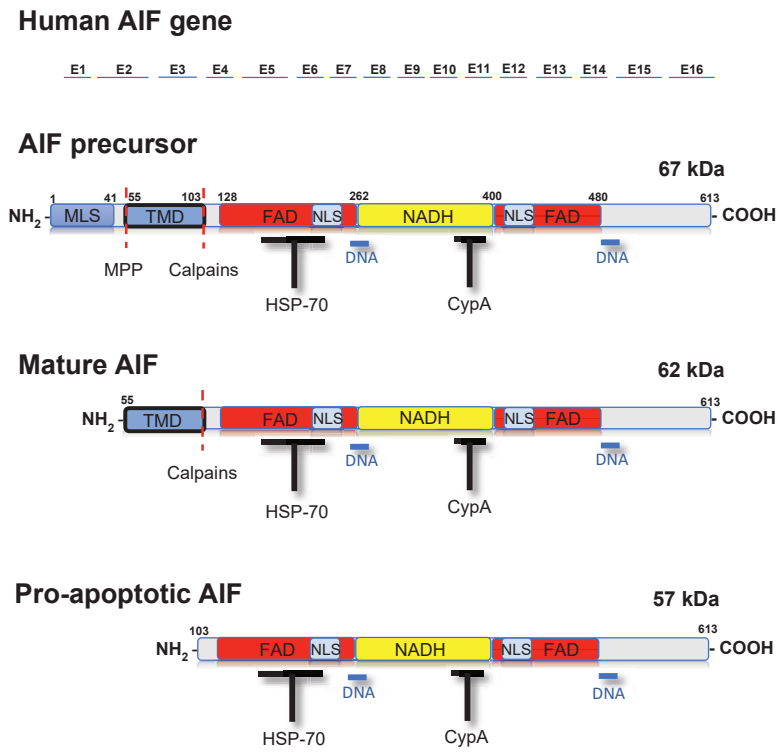

Figure 1. *Schematic representation of the different human AIF forms and their binding domains. Shown are the exons of the AIF gene (E1-E16) and the N-terminal, MLS, TMD, FAD, NLS, NADH and C-terminal domains, together with the HSP-70, DNA and CypA biding sites of the different AIF protein forms. MPP and calpains cleavage sites are also revealed.*

AIF is a highly conserved protein, and it has significant homology with the oxidoreductases of bacteria, plants, and fungi [66]. Therefore, it is not surprising that there is a high degree of preservation (92% AA identity) between human AIF and mouse AIF [67]. Human *AIF* is located at the q26.1 region of the X chromosome, while mouse *Aif* is located in region A6, also in the X chromosome.

In the absence of apoptotic stimuli, AIF is essential for obtaining energy in the mitochondria, as well as for the optimal functioning of the respiratory chain [68], making AIF an essential protein for survival [69]. AIF involvement in free radical formation and removal has also been suggested [70; 71]. In addition, some studies have suggested a relationship between AIF's redox function with the biogenesis and/or assembly of complexes I and III of the electron transport chain during oxidative phosphorylation (OxPhos), as well as with the maintenance of these complexes for optimum performance [72; 73]. In the presence of apoptotic stimuli, AIF plays a central role in neuronal cell death [46; 74]. In 2003, Zhu and colleagues found that AIF was involved in neuronal death after HI in the neonatal rat brain [75]. In that paper, they showed that AIF was detected in the nuclei just a few hours after HI and only in damaged areas. Furthermore, the larger the infarct volume, the greater the number of AIF-positive nuclei were found, and treating the mice with a multi-caspase inhibitor did not alter the number of AIF-positive nuclei [75; 76]. We know now that after HI AIF is cleaved from the IMM by calpains and/or cathepsins in its apoptotic form (Figure 1) [52; 77], with a molecular weight of 57 kDa [65]. The protein refolds while incorporating FAD and is then released into the cytosol, where it combines with CypA and the complex translocates to the nucleus [78]. Arthur and colleagues subsequently found that once in the nucleus, AIF also interacts with H2A histone family member X (H2AX) [79]. H2AX function is linked to DNA damage repair by modifying the chromatin structure and making damaged DNA sites accessible to repair factors [80]. The AIF/H2AX complex improves DNA accessibility to AIF [81], thus making the synchronized presence of these three proteins a team with specialized roles: AIF (binding domains), H2AX (generation of DNA accessibility), and CypA (DNase activity) [79]. Therefore, this set of molecules in the nucleus acts as a DNA degradation complex and is required for the large-scale DNA fragmentation and chromatinolysis (condensation of chromatin in the nuclear periphery) and leads ultimately to cell death in a caspase-independent manner. Chromatinolysis mediated by H2AX has also been observed in caspase-dependent apoptosis, in which the DNA degradation is of a different nature (oligonucleosomal instead of large-scale DNA degradation), and this could be because of the different actors implicated: Caspase 3/Caspase-activated DNase or AIF/CypA, respectively [79].

As mentioned above, the apoptotic mechanisms (including AIF translocation) are upregulated in the developing brain and play an important role in early neuronal development. Interestingly, it has been found that there is a relative downregulation of AIF with age (AIF was found at a constant level, but there were increased levels of mitochondrial markers, meaning that the relative abundance of AIF was reduced) with the exception of the cerebellum, in which

AIF protein was found to be increased with age [59]. On the contrary, autophagy was more pronounced in adult brains, and calpains showed no obvious developmental differences [59]. Surprisingly, together with a more prominent apoptotic mechanism in the immature brain, it was also found that juvenile mouse brains seem to have a greater capacity for regeneration after injury than immature mouse brains [82]. This conclusion was based on the fact that the juvenile hippocampus displayed a greater increase in neurogenesis compared to the immature hippocampus after HI, particularly in the sub-granular zone (SGZ) of the hippocampal dentate gyrus (DG). However, the juvenile levels after HI were not higher than the basal levels of the immature hippocampus under physiological conditions.

The importance of AIF in neuronal cell death after HI was confirmed when several experiments were carried out using 9-day-old Harlequin (Hq) mice, in which the level of expression of *Aif* was drastically reduced to 20% of the levels found in wild-type (WT) mice (leading to a 80% reduction of AIF protein levels) [83]. Hq mice were originally observed to undergo ataxia due to cerebellar atrophy as well as blindness due to retinal degeneration [71]. In Hq mice exposed to HI insult, the infarct volume after HI was reduced by 53% in male (YX^{Hq}) mice and by 43% in female ($X^{Hq}X^{Hq}$) mice. This also confirmed the independence of AIF from the caspase-dependent apoptosis pathway because the Hq mutation did not inhibit the release of Cyt c after HI, nor the activation of caspase 3, even though Hq mice displayed half the injury severity compared to WT mice. Furthermore, the combined protective effect of the Hq mutation, together with the administration of a caspase inhibition, reduced the infarct volume to more than 75%, showing that AIF and caspase act in parallel [83]. Hq mouse neurons were found to be particularly sensitive to oxidative stress-induced (by hydrogen peroxide (H_2O_2)) cell death, which suggested that AIF indeed acts as a mitochondrial scavenger of ROS and/or that AIF is involved in OxPhos. Neonatal Hq mice also exhibited 18% less respiratory chain complex I and 30% less catalase compared with WT mice. Finally, when the Hq mice were administrated an anti-oxidant agent (edaravone), the infarct volume was even more reduced compared to the reduction seen in Hq mice alone (~75% reduction vs. ~50% reduction), and was much more reduced than when edaravone was administrated to WT mice (~20% reduction in infarct volume). This was attributed to the fact that edaravone restored the anti-oxidant defense compromised by the Hq mutation [83].

1.4.1 AIF ISOFORMS

Recent studies have shown the existence of more variants of AIF (Figure 2). AIF2 contains 609 AAs (608 AAs in mice) and it expresses an alternative exon (2b) compared to the other isoform [84]. In opposition to AIF1 (which is

ubiquitously expressed), AIF2 is only expressed in the brain [85]. It has been shown that AIF2 is also found in the IMM, but as a result of the alternative splicing of exon 2 (which introduces a short difference in the second MLS of the protein), the segment that is used to anchor the protein into the IMM does so more firmly due to changes in the hydrophobicity of the AAs compared to the other isoform [85].

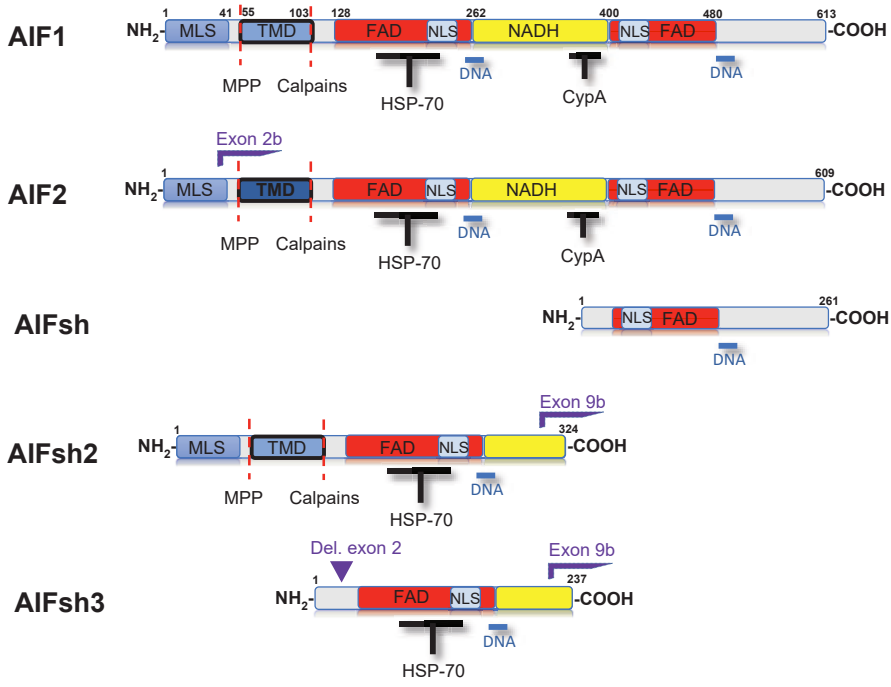

Figure 2. *Schematic representation of all AIF forms and their domains (MLS, TMD, FAD, NLS and NADH domains, together with the HSP-70, DNA and CypA biding sites). MPP and calpains cleavage sites are also revealed. The difference in the color intensity of the TMD domain of AIF2 reflects the alternative usage of exon 2b, affecting to the TMD segment. AIFsh2 and AIFsh3 are generated by the alternative splicing of the exon 9b. AIFsh3 has a similar structure as AIFsh2, but with the deletion of exon 2, which leads to the loss of MLS and TMD domains.*

AIFsh is produced from an alternative origin of transcription located at intron 9 of the *AIF* gene. As a result, AIFsh contains the C-terminal AIF domain encoded by exons 10 to 16, lacking of MLS. AIFsh is a cytosolic protein that causes the same apoptotic effects as AIF1 but lacks oxide-reductase function [86]. Two other human isoforms have also been discovered: AIFsh2 and AIFsh3 [87], generated by alternative splicing of the exon 9b. AIFsh2 contains AAs 1–324, while AIFsh3 is formed by AAs 87–324, meaning that both lack

the C-terminal and NLS2 domains and therefore they are not translocated into the nucleus. In addition, AIFsh3 also lacks the MLS sequence, due to the splicing of exon 2, and therefore the protein is not translocated into the mitochondria (Figure 2).

1.4.2 SUMMARY OF THE BREAKTHROUGH DISCOVERIES ABOUT AIF

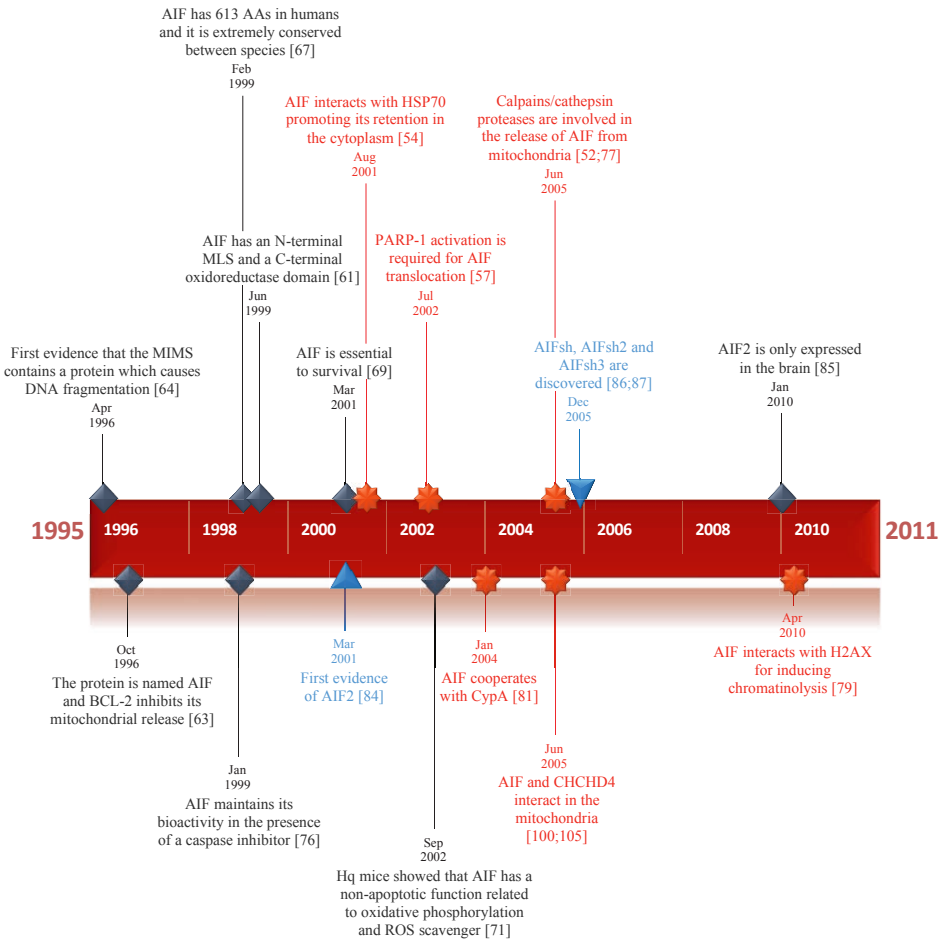

Figure 3. *Timeline with the breakthrough discoveries about AIF since its first evidence in 1996. Different colors and symbols were used based on the kind of event: general biological information discovered (black-diamond); new isoform discovered (blue-triangle), new protein interaction discovered (red-star 8 point).*

1.5 OXIDATIVE STRESS

Free radicals are formed in the brain as a consequence of the HI insult and reperfusion process, and they are implicated in the development of perinatal brain injury [88; 89]. When the amount of free radicals overcomes the antioxidant capacity of the cell, the excessive production will lead to oxidative stress [90] that will affect different macromolecules, including lipids, proteins, and nucleic acids. The neonatal brain is especially vulnerable to this damage due to its low concentrations of antioxidants in oligodendrocyte precursors compared to mature oligodendrocytes [43; 91; 92]. Among the most common free radicals generated are ROS, NO produced by neuronal NO synthase, and H_2O_2, which is produced by impaired glutathione peroxidase. The accumulation of all these free radicals plays an important role in apoptosis because they play a fundamental role in mitochondrial permeabilization and therefore in the release of mitochondrial intermembrane pro-apoptotic proteins to the cytosol [41].

Mitochondria, and especially mitochondria in brain cells, are also crucial in the development of oxidative stress because their energy demands are high and they are thus a major source of free radical production [93]. The consequences of such stress will negatively affect the metabolic processes taking place in mitochondria leading to a decrease in ATP production.

As previously explained, besides its participation in the mitochondrial apoptotic pathway, AIF also plays a crucial role in mitochondrial energetic functionality, especially concerning the maintenance of electron transport chain complexes I and III during OxPhos. The AIF oxidase-reductase activity was suggested by *in vitro* experiments performed using natural AIF purified from mitochondria that exhibited NADH oxidase activity while generating superoxide anions (O_2^-) [94].This activity was shown to be independent from its role in apoptosis because a recombinant AIF form lacking the FAD domain and therefore its NADH oxidase activity did not lose its apoptotic function [94]. In addition, the AIFsh isoform showed apoptotic activity despite lacking oxide-reductase activity [86], while AIFsh2 retained oxide-reductase activity despite lacking apoptotic activity [87]. A similar experiment was replicated some years later suggesting that AIF is a redox-signaling molecule in which its pro-survival and its pro-apoptotic roles are controlled by NADH [95]. Furthermore, it was pointed out that NAD^+ reduction would cause a transition in AIF protein from monomeric to dimeric form, and moreover that AIF dimerization could potentially lead to a conformational change in the protein affecting the accessibility of the NLS2 binding domain and DNA binding sites [96].

This property of AIF to form dimers also plays an important role when it comes to explaining some of the results obtained in one of our experiments regarding the *Aif2* KO paper. The idea behind this is that because AIF2 is, as previously mentioned, anchored more deeply into the IMM, and because AIF1 and AIF2 can form monomers or dimers (including heterodimers of AIF1/AIF2), AIF2 might have the ability to "kidnap" AIF1 by forming heterodimers and thereby affecting its capacity to translocate from mitochondria to the cytosol, as well as its oxidoreductase activity. Under apoptotic conditions there is usually a decrease in the mitochondrial levels of NADH. The fact that these transition forms (monomers or dimers) are related to the oxidative stress as well, in which the reduction with NADH causes a transition from monomer to dimer, might explain an evolutionary way to regulate the dual function of AIF during the first embryonic stages in the brain. All of this would indicate that the apoptotic function of AIF can be modulated by changes in NADH levels [95; 96; 97].

1.6 SEX DIFFERENCES

Sex differences in perinatal brain damage have been previously reported in different studies. As mentioned before, PARP-1 is a nuclear enzyme involved in DNA repair, but it is also involved in a unique PARP-1–dependent cell death program when the DNA damage is severe [98], and it is closely linked to AIF during the apoptotic process after acute neurological insults [57]. Some years ago, in a *Parp-1* study, it was found that the KO of this gene provided significant protection overall in the group of mice. However, analysis by sex revealed that males were strongly protected in contrast to females in which there was no significant effect [99]. When Cyt c is released from the mitochondria, it will activate caspase 3, which will translocate to the nucleus and cleave PARP-1, inactivating this protein and triggering caspase-dependent cell death. Based on the analysis of the cell death mechanisms, it has been shown that, at least in neuronal cell cultures, the caspase-independent pathway is more predominant in males and, in contrast, the caspase-dependent pathway is more prevalent in females [100; 101]. Sex differences have also been reported for TH, resulting in more effective long-term protection in female than in male 7-day-old rats [102]. Autophagy has been suggested to show sexual dimorphism based on the fact that females have greater basal autophagy activity [103]. Furthermore, while there was no sex difference in brain injury at any age when the HI insult was severe, when the insult was moderate, adult (60 days old) male mice displayed more severe injury compared to females [101]. Taken together, these results lead us to the conclusion that mitochondria are the central reason for the sexual dimorphism in the HI response [104].

2 AIM

The hypothesis of this project is that AIF plays a fundamental role in mitochondrial regulation in brain injury after HI, not only by the loss of its energy-producing function, but also by its release to the cytosol and consequent translocation to the nucleus, where AIF will lead to chromatin condensation and large-scale DNA fragmentation. In order to achieve this goal, the project has been divided into four independent but related studies (Figure 3).

1. To study the effect of coiled-coil-helix-coiled-coil-helix domain-containing protein 4 (CHCHD4) haploinsufficiency in the brain injury process and its interaction with AIF (**paper I**).

It has previously been reported that low levels of AIF lead to low levels of CHCHD4 protein (without affecting the mRNA level) [100]. Furthermore, high levels of CHCHD4 have been shown to help offset the problems associated with low levels of AIF, and low levels of CHCHD4 have been shown to lead to similar problems as low levels of AIF [100; 105]. All of these results suggest that both proteins work epistatically, at least in terms of mitochondrial regulation. Therefore, we decided to investigate whether low levels of CHCHD4 were associated with reduced severity of brain injury.

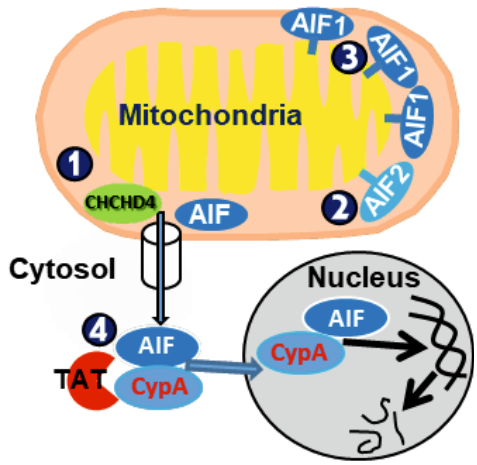

Figure 4. *Representative image of all the studies of this project. The numbers represent the four different studies described in the text. Study 1: to study the effect of chchd4 haploinsufficiency and its interaction with AIF and other proteins in the IMS. Study 2: to characterize the newly discovered isoform AIF2. Study 3: to analyze the effect of Aif overexpression. Study 4: to study the pharmacological inhibition of the AIF/CypA complex.*

2. To characterize the newly discovered AIF2 isoform (**paper II**).

Numerous functional studies have been performed on AIF1, the most abundant and ubiquitous AIF isoform, whereas AIF2 has not been further characterized. The aim of this study was to assess for the first time the functional and regulatory profiling of AIF2, by studying the consequences of *Aif2* KO on the brain and development of brain injury after HI insult in mouse pups.

3. To investigate the results of a newly generated transgenic mouse in which Aif is overexpressed (**paper III**).

This model was made by combining the original *Aif* located on the X chromosome together with a knock-in (KI) *Aif*. The effects of *Aif* overexpression under both physiological conditions and after HI have never been studied before. The hypothesis in this study was that AIF up regulation increases the severity of brain damage after HI insult. Furthermore, because the *Aif* gene is located on the X chromosome and is therefore an X-linked gene, changes in AIF expression might show differences by sex under physiological and/or pathological conditions.

4. To analyze the effects of a peptide that inhibits the apoptotic effect of AIF without affecting its pro-survival features (**paper IV**).

Under apoptotic stimuli, AIF translocates from the mitochondria to the nucleus, but in order for this to happen AIF requires the interaction with CypA in the cytosol prior the translocation to the nucleus. A recent study showed that the AIF/CypA complex presents a good target for generating pharmacological inhibitors that block the cell death process [38]. A peptide was designed (AIF370–394) based on the AIF and CypA sequences that correspond to the surfaces involved in binding. This molecule acts as a cell-penetrating peptide by using the trans-activator of transcription (TAT) sequence (GRKKRRQRRRPQ), which has been a very successful way to overcome the lipophilic barrier of the cellular membranes and to deliver molecules inside the cell [106; 107]. *In vitro* experiments have already demonstrated the efficacy and protective effect of the peptide [108]. The purpose of this study was to determine if the blocking peptide has neuroprotective effects *in vivo*.

Overall, the main aim of this PhD project is that a better understanding of the role of AIF in HI brain injury will help in developing better and more effective treatments during the early stages of brain injury.

3 MATERIALS AND METHODS

3.1 ANIMALS

For all our experiments, we used mice from the strain C57BL/6 or transgenic mice on C57BL/6 background, which have an intermediate sensitivity to HI compared to two other commonly used strains, 129Sv and CD1, which are highly resistant and highly susceptible to HI insult, respectively [109]. Mice were maintained in the Laboratory for Experimental Biomedicine (EBM), Sahlgrenska Academy, University of Gothenburg, Sweden. All animals were housed in a controlled temperature and pathogen-free environment under a 12:12-hour light–dark cycle, and all experiments were approved by the Animal Ethics Committee of Gothenburg (90-2011, 111-2014 and 112-2014). For the breeding of new pups, two females and one male with the desired genotype were placed together in one cage with access to water and food and in appropriate conditions of temperature and air. The pups remained in the parents' cage for approximately 21 days, at which time the mice were transferred to independent cages and separated into males and females.

In order to achieve our goals, different transgenic mice were generated for each study (except in study IV that C57BL/6 mouse pups were used), as well as a specific methodology.

I. ***Chchd4*** **haploinsufficiency study:** *Chchd4* heterozygous breeding mice were obtained from the animal facility of Gustave Roussy, France, through collaboration with Dr. Nazanine Modjtahedi, and bred at the Laboratory of Experimental Biomedicine of University of Gothenburg, Sweden. Postnatal day (P)9 WT and heterozygote *Chchd4* KO littermates of both sexes were subjected to HI, and mice were sacrificed at different time points (6 h, 24 h, 72 h, and 4 weeks post-HI) and their brains were removed in order to evaluate the extent and development of brain damage over time.

II. ***Aif2*** **PGK-Cre KO study:** For this study, we generated *Aif2* KO C57BL/6 mice by using Cre/loxP technology. In order to generate this mouse, two different strains were used. The first had a transgene expressing the Cre recombinase (a site-specific integrase isolated from the P1 bacteriophage that catalyzes recombination between two of its consensus DNA

recognition sites) under the control of the phosphoglycerate kinase (PGK) promoter, meaning that it was ubiquitously expressed [110]. The second strain had the LoxP sites flanking exon 2b of the *Aif2* gene (generated by Ozgene, Australia). In this system, both LoxP sites are 34 bp and contain two 13 bp palindromic sequences in trans orientation that flank a spacer region of 8 bp. When a mouse with the PGK-Cre is bred with an *Aif2* floxed strain, the Cre protein will recognize and bind to the 13 bp palindromic regions forming a dimer. This subsequently binds to the dimer of the second LoxP site forming a tetramer. The strands are then cut by the Cre protein and rejoined by DNA ligase. This event results in a frameshift generating a null allele, and the *Aif2* gene will not be expressed. Cre/LoxP technology is commonly used because it allows knock out of genes in an inducible way. The LoxP sites can also be placed in a cis orientation (which invert the intervening sequence) or can be located on different chromosomes (which generate a translocation), and this in combination with different kind of promoters (like tissue-specific promoters) makes this technology a very versatile tool for researchers. P9 mice were subjected to HI and sacrificed and had their brains removed at different time points (6 h, 24 h, and 72 h post-HI). Adult mice were also used in order to evaluate neurogenesis and their performance on behavioral tests under physiological conditions.

III. ***Aif* overexpression study:** For this study, we wanted to study the effect of overexpressing *Aif* by adding an exogenous *Aif* gene using a newly generated unique transgenic mouse strain. The model consists of a Cre-regulated KI strain using the Rosa26 KI vector. Rosa26 acts as a "stopper" between the promoter and the gene. By using Cre technology, Rosa26 can be removed leading to the expression of the gene that would otherwise be inhibited. The floxed mice were crossed with actin-Cre mice that were obtained from Jackson Laboratories. This model generated transgenic mice with up-regulated *Aif*. Two different genotypes of this transgenic mouse were generated: $Aif^{flox/+}$–actin-cre (KI) and $Aif^{+/+}$–actin-cre (WT) mice. HI was performed on P9 mice, and brain samples were collected when the pups were sacrificed at 24 h and 72 h post-

HI in order to evaluate the effect of the overexpression under both pathological and physiological conditions.

IV. **Pharmacological inhibition of the AIF/CypA complex:** C57BL/6 mouse pups together with their mother were delivered from Janvier Labs (Le Genest Saint Isle, France). On P9 pups were subjected to HI. Before surgery involving the ligation of the carotid artery, all the pups received, while they were awake, an intranasal dose of 1.5 μL of hyaluronidase (100 U, Sigma-Aldrich, St. Louis, MO, USA) in phosphate-buffered saline (PBS) to each nostril and spontaneously inhaled. Immediately after that, half of the pups were treated (also via intranasal administration) with 1.5 μL of AIF(370-394)-TAT (at a concentration of 10 μg/μL). The other half of the mice were treated with PBS and used as control mice. This procedure was repeated immediately prior to hypoxia again (but this time only peptide/PBS was administrated, not the hyaluronidase). The mice were sacrificed by decapitation 8 h or 12 h post-HI and the brains were extracted immediately after perfusion. These mice were used for immunohistochemistry (AIF, caspase 3, and Fluoro-Jade) and proteomic analysis, and they were all males. Another set of mice (this time of both sexes) were used for brain injury analysis using microtubule-associated protein 2 (MAP2) and myelin basic protein (MBP) immunohistochemistry analysis in order to study grey matter and white matter injury, respectively. For this purpose, the mice were treated as before, but the AIF(370-394)-TAT peptide was also administrated at 12 hours after HI. At 72 h after HI, the mice were sacrificed by decapitation and the brains were extracted after the perfusion.

3.2 HI MODEL

The most widely used model of neonatal HI is the Rice–Vannucci model using P7 rats [39; 111] and its adaptation for use with P7mice [109]. At 5, 9, 21, and 60 days of age, mice correspond to preterm, term, juvenile, and adult humans, respectively. In this PhD project, P9 mice of both sexes were used for HI experiments.

Pups were anesthetized with isoflurane (5% for induction, 1.5% to 2.0% for maintenance) in a 1:1 mixture of nitrous oxide and oxygen, and the surgery was completed in less than 5 min in order to avoid side effects from the anesthesia [112]. The left common carotid artery was cut between double ligatures of Prolene sutures (6.0). After the surgical procedure, the wounds were infiltrated with lidocaine for local analgesia. The pups were returned to their cages for 1 h and then placed in a chamber perfused with a humidified gas mixture (10% oxygen in nitrogen) for 50 min at 36°C. The animals were kept in the chamber in humidified air at 36ºC for 10 minutes before and 10 minutes after the hypoxic exposure. During this time, cerebral blood flow is reduced by 40%–60% in the hemisphere ipsilateral (IL) to the ligation [39]. Although, there is a compensatory vasodilatation of the vessels in the contralateral (CL) hemisphere, this cannot counterbalance the effect of the ligated hemisphere resulting in hypoxia and ischemia. Following hypoxic exposure, the concentration of oxygen in the chamber was restored to normal values for 10 min and then the pups were returned to their home cages.

The brain damage incurred in this model is restricted to the IL hemisphere, leaving the CL hemisphere unaffected for use as an internal control [113]. Animals that survived the insult (in our case, approximately 80%–90% of the mice subjected to this model) generally lived as long as normal animals.

3.3 GENOTYPING (I, II & III)

Knowing the genotypes of the mice is crucial when there are different strains in the same experiment (KO, KI, WT, and haploinsufficient mice among all the studies). For genotyping, genomic DNA was isolated from about 3 mm of tissue from the tail, and according to the manufacturer's instructions (DNeasy 96 Blood & Tissue Kit, 69506, Qiagen, Hilden, Germany) the samples were incubated in 180 µL of digestion-buffer ATL together with 20 µL of proteinase K (Qiagen, Hilden, Germany) overnight at 56ºC. The DNA was afterwards purified, extracted, and the final product eluted with 200 µL of AE buffer, and the DNA concentration was measured using a Nanodrop (Thermo Scientific, USA).

Polymerase chain reaction (PCR) was performed on a Biometra T3 thermocycler (Biometra GmbH, Göttingen, Germany) using different sets of primer pairs depending on the study. A total of 1 µl of the resulting purified DNA was used together with 0.2 mM deoxyribonucleoside triphosphates (dNTPs), 4 µl 5× SYBR Green PCR buffer (250 mM Tris-HCl, pH 8.3, 375 mM KCl, 15 mM $MgCl_2$; Promega) and 1 U of Taq DNA Polymerase (Promega) and 0.5 µM of the appropriate primers. Afterwards, the PCR

products were separated on a 1.5% agarose gel electrophoresis system (Bio-Rad, California, USA) containing SYBR Green (1:10,000 dilution). A 100 bp or a 1000 bp ladder was used to verify the sizes of the PCR products. The gels were imaged with a LAS 3000 cooled CCD camera (Fujifilm, Tokyo, Japan).

All the different studies had specific considerations due to the unique strains that were used.

I. ***Chchd4* haploinsufficiency study:** The following primers (IST11943B12-r) were used.

***Chchd4* haploinsufficiency study**			
Genotype	**Primer (forward)**	**Primer (reverse)**	**Segment size amplified**
WT	5'-GTG CTC CTC ATA GGG ATC ATT GG-3'	5'-TGG GCT GGT TAG TCA GTG ATT GG-3'	213 bp
Mutant	5'-GTG CTC CTC ATA GGG ATC ATT GG-3'	5' -AAA TGG CGT TAC TTA AGC TAG CTT GC-3'	205 bp

II. ***Aif2* PGK-Cre KO study:** PCR was performed using four different primer pairs.

***Aif2* KO study**			
Target	**Primer (forward)**	**Primer (reverse)**	**Segment size amplified**
P1/P2	5'-TTG GGG ATA GGG TGG GTA AGA C-3'	5'-GAG GTA ACA AAA GGG ACA CTG CC-3'	518 bp from the WT allele, 2377 bp from the flox allele, and 637 bp from the flox Δ-neo allele
P3/P2	5'-GAG GTA ACA AAA GGG ACA CTG CC-3'	5'-GAA AGC GAA GGA GCA AAG CTG-3'	836 bp from the flox allele
P4/P2	5'-GAG AAC AAA AGG TTG GAT GCC AC-3'	5'-GAA AGC GAA GGA GCA AAG CTG-3'	1062 bp from the WT allele and 568 bp from the KO allele
PGK-cre	5'-GCA AGC TTT CGA CCA TGC CCA AGA AGA AG-3'	5'-GCG AAT TCC GTT AAT GGC TAA TCG CCA TC-3'	380 bp from the cre allele

III. ***Aif*-overexpression study:** The following primers were used.

***Aif*-overexpressed study**			
Genotype	**Primer (forward)**	**Primer (reverse)**	**Segment size amplified**
AIF flox	5'-GAG TTC TCT GCT GCC TCC TG-3'	5'-AAG ACC GCG AAG AGT TTG TC-3'	215 bp from the flox allele
AIF flox	5'-GAG TTC TCT GCT GCC TCC TG-3'	5'-CGA GGC GGA TAC AAG CAA TA-3'	322 bp from WT flox allele
β-actin-cre	5'-CTG CCA CGA CCA AGT GAC AGC AAT G-3'	5'-GCC TTC TCT ACA CCT GCG GTG CTA A-3'	326 bp from the cre allele

IV. **Pharmacological inhibition of the AIF/CypA complex:** For this study, genotyping was not necessary because all the mice for both groups were P9 C57BL/6J mice delivered from Janvier Labs, France. The only difference was that one group was treated with the AIF(370-394)-TAT peptide and the other group was treated with PBS and used as the control.

3.4 IMMUNOHISTOCHEMISTRY

3.4.1 TISSUE PREPARATION

At 6–8 h, 24 h, 72 h (or 4 weeks, for study I only) after HI-induced brain injury (time points depending on the study and on the type of experiment), the pups were deeply anesthetized by intraperitoneal administration of 50 mg/ml of sodium phenobarbital and intracardially perfusion-fixed with PBS and 5% buffered formaldehyde (Histofix; Histolab Products AB, Västra Frölunda, Sweden). Control animals were sacrificed accordingly at the same age (on P9, P12, or P38). The brains were rapidly removed and immersion-fixed in 5% buffered formaldehyde at 4°C for 18–24 h. Afterwards the brains were dehydrated in graded alcohol and xylene and embedded in paraffin. Coronal sections (5 μm) were cut throughout the brains, and before the histochemical procedures the sections were deparaffinized in xylene and rehydrated in graded alcohol, followed by antigen recovery by boiling in citric acid buffer (0.01 M, pH 6.0) for 10 minutes. Nonspecific binding was blocked for 30 min with 4% goat or horse serum (depending on the species used to raise the secondary antibody) in PBS.

After blocking, sections were incubated at 20°C for 60 min or overnight at 4°C with primary antibodies diluted in PBS (see list of monoclonal primary antibodies used below, categorized based on the different studies) and then incubated for 60 min with biotinylated secondary antibodies diluted in PBS, both of them at room temperature. Afterwards, the appropriate biotinylated secondary antibodies were added to each section for 60 min at room temperature (1:200 dilutions, except BLPN, which was 1:150); all from Vector Laboratories, Burlingame, CA, USA, expect for the 5-bromo-2-deoxyuridine (BrdU), which was from Jackson ImmunoResearch Lab, West Grove, PA, USA).

After blocking endogenous peroxidase activity with 3% H_2O_2, antigen staining was visualized by using an ABC Kit (1:200 dilutions, Vector Laboratories, Burlingame, CA, USA) for 60 min at room temperature along with 3,3'-diaminobenzidine enhanced with 15 mg/ml ammonium nickel sulfate, 2 mg/ml

beta-D glucose, 0.4 mg/ml ammonium chloride, and 0.01 mg/ml beta-glucose oxidase (all from Sigma, St Louis, MO, USA). After dehydrating with graded ethanol and xylene, the sections were mounted using Vector mounting medium.

For samples taken 72 h after HI, every 100th section throughout the whole brain was stained for MAP2 and MBP, and for the samples taken 6–8 h and 24 h after HI, every 50th section in the hippocampus level was stained for active caspase 3, AIF, 3-nitrotyrosine (3-NT), 8-hydroxyguanosine (8-OHG), doublecortin (DCX), Fluoro-Jade, BrdU, and brain lipid-binding protein (BLBP). The tables with the different kinds of markers are listed below.

***Chchd4* haploinsufficiency study**			
Protein	**Animal**	**Dilution**	**Company**
MAP2	Mouse	1:1000	clone HM-2, M4403, Sigma
BrdU	Rat	1:100	clone BU1/75, Oxford Biotechnology
AIF	Goat	1:100	sc-9416, Santa Cruz
BLPN	Rabbit	1:600	ABN14, Millipore
S-100β	Rabbit	1:1000	Swant, Bellinzona
NeuN	Mouse	1:200	clone: MAB377, Chemicon

***Aif2* KO study**			
Protein	**Animal**	**Dilution**	**Company**
MAP2	Mouse	1:1000	clone HM-2, M9942, Sigma
Cas-3	Rabbit	1:150	559565, BD Pharmingen
AIF	Goat	1:100	sc-9416, Santa Cruz Biotechnologies
3-NT	Mouse	1:200	ab53232, Abcam
8-OHG	Mouse	1:200	ab48508, Abcam

***Aif*-overexpression study**			
Protein	**Animal**	**Dilution**	**Company**
MAP2	Mouse	1:1000	clone HM-2, M4403, Sigma
MBP	Mouse	1:500	clone SMI94, 836504, BioLegend
Caspase-3	Rabbit	1:200	Asp175, 9661, Cell Signaling
AIF	Rabbit	1:500	E20, ab32516, Abcam
3-NT	Mouse	1:200	ab53232, Abcam
8-OHG	Mouse	1:200	ab48508, Abcam
DCX	Goat	1:500	C-18, sc-8066, Santa Cruz

Inhibition of AIF/CypA complex study			
Protein	**Animal**	**Dilution**	**Company**
MAP2	Mouse	1:1000	clone HM-2, M4403, Sigma
MBP	Mouse	1:400	clone SMI94, 836504, BioLegend
Caspase-3	Rabbit	1:300	Asp175, 9661, Cell Signaling
AIF	Rabbit	1:500	E20, ab32516, Abcam

3.4.2 GREY-MATTER INJURY EVALUATION

The brain injury was evaluated by immunostaining of MAP2 using Micro Image software (Olympus, Japan) and calculating the infarct volume and injury score in different brain regions (cortex, hippocampus, thalamus, and striatum). MAP-2 is part of the cytoskeleton in neurons (including dendrites and soma) and proximal axons. In the neonatal brain, loss of MAP-2 staining corresponds well to areas of brain injury and therefore to infarction in gray matter.

- **Tissue loss**

The volume of tissue loss was calculated according to the Cavalieri Principle, which states that the volume of two or more irregularly shaped objects is the same if those objects have the same cross-sectional area at every level and the same height. In other words, the volume of a figure can be estimated from a set of two-dimensional slices throughout the figure. In the formula $V = \Sigma Apt$, V is the total volume expressed as mm^3, ΣA is the sum of the areas measured, p is the inverse of the section's sampling fraction, and t is the section thickness (5 μm). This provided the sum of the infarction volume and the total tissue volume loss. The total hemispheric tissue loss was calculated as the MAP2-positive volume in the CL hemisphere minus the MAP2-positive volume in the IL hemisphere. The infarction volume was equal to the MAP2-negative volume in the IL hemisphere. The tissue loss of both hemispheres was measured by using Micro Image (Olympus, Japan) for the first study and ImageJ 1.52a software (NIH, Bethesda, MD, USA) for studies II, III, and IV.

- **Neuropathological score**

Neuropathological score was used as a complement to total tissue loss, but it is also a good tool for evaluating the injury in specific brain regions (cortex, hippocampus, striatum, and thalamus). It was assessed by using a semi-quantitative neuropathological scoring system [114]. The cortical injury was graded from 0 to 4 with 0 being no observable injury and 4 being confluent infarction encompassing most of the cerebral cortex. The damage in the hippocampus, striatum, and thalamus was assessed both with respect to hypotrophy (shrinkage) (score 0–3) and observable cell injury/infarction (score

0–3) resulting in a neuropathological score of 0–6 for each brain region. The total score was the sum of the scores for all four regions, resulting in a total possible score of 22. The neuropathological score evaluation and volume measurements were carried out by investigators blinded to group assignment.

3.4.3 SUBCORTICAL WHITE MATTER INJURY (III, IV)

The white matter of both hemispheres was measured using MBP staining, which is a major constituent of the myelin covering of oligodendrocytes in the central nervous system, and therefore an indicator of developing oligodendrocytes and myelin.

The white matter of both hemispheres was measured using ImageJ 1.52a software (NIH, Bethesda, MD, USA). For all the MBP calculations, only the subcortical areas were included for both hemispheres, and three consecutive sections on the same level for each animal were calculated and averaged as the final ratio. The final score was calculated as follows: ((CL hemisphere − IL hemisphere) / CL hemisphere) × 100%.

3.4.4 CASPASE 3 (II, III & IV), AIF (I–IV), 3-NT (II & III) AND 8-OHG (II & III) STAINING

Caspase 3 has already been mentioned as one of the key executors of the caspase-dependent apoptotic cell death, and caspase 3 activation is required for this pathway. AIF is the key executor of the caspase-independent apoptotic pathway and is translocated to the nucleus upon activation. The immunohistochemistry analysis was performed in a similar way as previously explained for the MAP2 staining, but using the specific primary and secondary antibodies listed above. The caspase 3-positive cells and AIF-positive nuclei were counted in the four different brain regions analyzed (cortex, striatum, nucleus habenularis (NH), and cornu ammonis 1 (CA1)), and then averaged for all the sections in each brain.

3-NT and 8-OHG are both markers of oxidative stress. While 8-OHG is a marker of oxidative damage in the nucleic acids, 3-NT is used to study oxidation in proteins because it is a stable marker of peroxynitrite formation and thus indicates protein nitrosylation.

3.4.5 FLUORO-JADE STAINING (I, IV)

For Fluoro-Jade staining, the procedure was similar as previously described, but after the rehydration (100% alcohol, 3 min; 70 % alcohol, 1 min; distilled water, 1 min) the brain sections were incubated in 0.06% potassium permanganate ($KMnO_4$) for 15 min at room temperature in a shaker. Following

a wash in distilled water for 1 min, the samples were stained with 0.0004% Fluoro-Jade B (2210364, Temecula, CA, USA) in 0.09% acetic acid for 30 min in the dark. The sections were then washed again in distilled water two times (1 min each) and cover slipped and kept in the dark.

3.4.6 BRDU ADMINISTRATION (I)

The thymidine analog BrdU (Roche, Mannheim, Germany, 5 mg/mL dissolved in 0.9% saline) was prepared fresh immediately prior to use and injected intraperitoneally (50 mg/kg) into P10 and P11 mice. The mice were sacrificed four weeks after the injection (at P38) in order to evaluate the survival of newly proliferated cells.

The phenotype of BrdU-labeled cells was determined using antibodies against neuronal nuclei (NeuN) to detect mature neurons and antibodies against S-100β to detect astrocytes. Antigen recovery was performed as mentioned above for the immunohistochemistry tissue preparation, and this was followed by incubation with the specific antibodies provided in the list above (BrdU together with mouse NeuN, and S-100β) diluted in PBS at 20°C for 60 min. After washing, the sections were incubated with the secondary antibodies Alexa Fluor 488 donkey anti-rat IgG (Heavy + Light chain, (H+L)), Alexa 555 donkey anti-mouse IgG (H+L), and Alexa 647 donkey anti-rabbit IgG (H+L) (all diluted 1:500 and from Jackson ImmunoResearch Lab, West Grove, PA, USA) at 20°C for 60 min. After washing, the sections were mounted using Vectashield mounting medium.

3.4.7 IMMUNOFLUORESCENCE STAINING (III)

For the immunofluorescence staining, the deparaffinization, rehydration, and antigen recovery were performed as described above. After blocking with 4% donkey serum in PBS for 30 min, the mixed primary antibodies of monoclonal anti-AIF and monoclonal mouse anti-FLAG (both listed below) were incubated with the sections overnight at 4°C. After the primary antibody incubation, the mixed secondary antibodies of donkey anti-rabbit Alexa Fluor 488 (1:500 dilution, A21206, ThermoFisher Scientific, Waltham, MA, USA), and donkey anti-mouse Alexa Fluor 555 (1:500 dilution, A31570, ThermoFisher Scientific, Waltham, MA, USA) were added to each section for 120 min at room temperature. After washing, the sections were mounted on coverslips with ProLong Gold anti-fade reagent with DAPI (P36931, Invitrogen, Eugene, Oregon, USA). Representative images were taken at 200× magnification.

Aif-overexpression study			
Protein	**Animal**	**Dilution**	**Company**
AIF	Rabbit	1:500	E20, ab32516, Abcam
FLAG	Mouse	1:500	M2, F1804, Sigma

3.4.8 CELL COUNTING

The active caspase 3-positive cells, AIF-positive nuclei, 3-NT–positive cells, and 8-OHG–labeled cells were counted in every 50th section in an area contour with fixed locations at different magnifications, depending on the paper, within a defined area (one visual field) of the cortex, striatum, CA1, and NH using the ImageJ 1.52a software (NIH, Bethesda, MD, USA). Three sections were counted from each brain with an interval of 250 μm (5 μm × 50 sections).

The numbers of Ki-67–positive and DCX-positive cells were counted in the SGZ of the DG in three adjacent sections in the hippocampus. The length of the SGZ was measured, and the number of positive cells was expressed as the number per mm. The average was defined as 1 mm when comparing different brains.

The AIF-labeled or Fluoro-Jade–labeled cells were counted in the border zone of the cortical infarcts at 400× magnification. Three sections were counted, each of them 50 sections apart, and expressed as the average number of cells per visual field.

The numbers of BrdU-labeled and BLBP-labeled cells were counted in every 50th section throughout the granule cell layer and the SGZ (for BrdU) or the SGZ only (for BLBP) using a stereomicroscope (StereoInvestigator, MicroBrightField Inc., Magdeburg, Germany), and at least six sections were counted from each sample. For the phenotype of BrdU-labeled cells, at least 50 BrdU-positive cells in the DG were counted using a confocal laser scanning microscope (Leica TCS SP, Heidelberg, Germany), and the ratio of BrdU/NeuN and BrdU/Glial fibrillary acidic protein (GFAP) double-labeled cells was calculated for each sample. The total number of newborn neurons ($BrdU^+/NeuN^+$) and astrocytes ($BrdU^+/GFAP^+$) in each sample was calculated based on the number of BrdU-positive cells and the ratio of double labeling. All counting was carried out by investigators blinded to the group assignment.

3.5 RNA ISOLATION, CDNA SYNTHESIS, AND RT-QPCR (I, II & III)

Total RNA was isolated using the RNeasy Mini kit (Qiagen, 74104) according to the manufacturer's instructions. The concentration and purity of all RNA samples was determined using a Nanodrop spectrophotometer (Nanodrop Technologies, Wilmington, USA), and the integrity of the RNA was measured using an Experion RNA StdSens analysis kit (7007103, Bio-Rad, Hercules, California, USA) on an automated electrophoresis station (Bio-Rad, Hercules, California, USA). One microgram of total RNA was reverse transcribed using the QuantiTect Reverse Transcription kit (205311, Qiagen, Hilden, Germany). Quantitative reverse transcription PCR (RT-qPCR) was performed using a LightCycler 480 instrument (Roche Diagnostics, Mannheim, Germany) and the SYBR green (0253, ThermoFisher Scientific, Waltham, MA, USA) technique according to the manufacturer's instructions.

The primers used in the RT-qPCR reactions were designed by Beacon Designer software (PREMIER Biosoft, CA, USA). The relative expression levels of mRNAs were calculated by the method of geometric averaging of multiple internal control genes according to the formula of $2^{-(\Delta\Delta CT)}$ [115; 116].

The isolated RNA was used for different purposes depending on the study.

I. ***Chchd4*** **haploinsufficiency study**

The primers used in the RT-qPCR reactions were designed to study the mitochondrial biogenesis, fission-fusion, Keap-NRF2 pathway-related, and p53 pathway-related gene expression. The names of the genes with the sense and antisense primers used are presented in the following table.

Chchd4 haploinsufficiency study			
Gene	**Sense**	**Antisense**	**Function**
Pgc-1α	5'-CCA GGT CAA GAT CAA GGT-3'	5'-CGT GCT CAT AGG CTT CAT A-3'	mitochondrial biogenesis
Tfam	5'-ACC TCG TTC AGC ATA TAA CAT T-3'	5'-ATC ACT TCG TCC AAC TTC AG-3'	mitochondrial biogenesis
Nrf1	5'-CCA CAG GAG GTT AAT TCA GAG-3'	5'-ACA TCA CTG CGG ACA TTG-3'	mitochondrial biogenesis
Drp1	5'-TGC TCA GTA TCA GTC TCT TC-3'	5'-GGT TCC TTC AAT CGT GTT AC-3'	mitochondrial fission
Fis1	5'-ATG AAG AAA GAT GGA CTG GTA G-3'	5'-GGA TTT GGA CTT GGA GAC A-3'	mitochondrial fission
Mff	5'-ATT CAA TCA CTG TAG CGT TCT-3'	5'-CTT TAT ATT TCC AGG TGT TGA GAC-3'	mitochondrial fission
Opa1	5'-CCT GTG AAG TCT GCC AAT-3'	5'-TTA GAG AAG AGA ACT GCT GAA AT-3'	mitochondrial fusion
Mfn1	5'-CAC TGA TGA ACA CGG AGA A-3'	5'-CGA CGG ACT TAC AAC CTT-3'	mitochondrial fusion
Mfn2	5'-CGC CAT ATA GAG GAA GGT-3'	5'-CGC ATA GAT ACA GGA AGA AG-3'	mitochondrial fusion
Gclc	5'- TAG AAC ACG GGA GGA GAG-3'	5'-CCA CAC TTA GAC AGG TAG C-3'	Keap-Nrf2 pathway
Keap1	5'-ATG GGA ATA AAG AAT GGA GTA GG-3'	5'-ATG GCA AGC AGA GAC AAT AG-3'	Keap-Nrf2 pathway
Nrf2	5'-GTG CTC CTA TGC GTG AAT-3'	5'-CGG CTT GAA TGT TTG TCT TT-3'	Keap-Nrf2 pathway
Ho1	5'-TAC ACA TCC AAG CCG AGA A-3'	5'-TAC AAG GAA GCC ATC ACC A-3'	Keap-Nrf2 pathway
p53	5'-ACA AGA AGT CAC AGC ACA T-3'	5'- CCA GAT ACT CGG GAT ACA AAT-3'	p53 pathway
p21	5'-AAG TGT GCC GTT GTC TCT-3'	5'-AAG TCA AAG TTC CAC CGT T-3'	p53 pathway
Peg3	5'-AAG GAA GAG GCG TTA CCA-3'	5'-TCA TCT CAG CAC CAC ACT-3'	p53 pathway
Usp7	5'-TGA GTG AGT CGG TCC TTA G-3'	5'-TGG AGT CAG ATT CAG CAT TG-3'	p53 pathway
Mdm2	5'-TGG CGT AAG TGA GCA TTC-3',	5'-GGC TGT AAT CTT CCG AGT C-3'	p53 pathway
PUMA	5'-GCG GAG ACA AGA AGA GCA G-3'	5'-AGG AGT CCC ATG AAG AGA TTG-3'	p53 pathway
Ywhaz	5'-CCT CAA CTT CTC TGT GTT CTA TT-3'	5'-ACG ACT CTT CAC TTA ATG TAT CAA-3'	Reference gene

II. *Aif2* PGK-Cre KO study

To confirm the expression of mitochondrial biogenesis, fusion and fission, and oxidative stress-related genes, RT-qPCR was performed as described above. However, in this study, we also studied the gene expression profiling of *Aif1*/*Aif2*, and for this purpose RNA was reverse transcribed using the TATAA GrandScript cDNA Synthesis Kit (TATAA Biocenter, Gothenburg, Sweden) in single 10 µl reactions containing 500 ng total RNA according to the manufacturer's instructions. All cDNA samples were diluted with nuclease-free water to a total volume of 100 µl. Quantitative real-time RT-qPCR was

performed with a CFX384 Touch real-time cycler (Bio-Rad, Hercules, CA, USA). Each 6 µl reaction contained 1× TATAA SYBR GrandMaster Mix (TATAA Biocenter, Gothenburg, Sweden), 400 nM of each primer, and 2 µl cDNA. The temperature profile was 95°C for 2 min followed by 40 cycles of amplification (95°C for 5 s, 60°C for 20 s and 70°C for 20 s). All samples were analyzed by melting curve analysis. Relative quantification using reference genes was applied. Twelve potential reference genes from the Mouse Reference Gene Panel (TATAA Biocenter, Gothenburg, Sweden) were evaluated with NormFinder, and *Actb* and *Pgk1* were chosen as the optimal reference genes.

***Aif2* KO study**			
Gene	**Sense**	**Antisense**	**Function**
AIF1	5'-CGA GCC CGT GGT ATT CGA-3'	5'-CCA TTG CTG GAA CAA GTT GC-3'	Apoptosis
AIF2	5'-CGA GCC CGT GGT ATT CGA-3'	5'-CTA GGA GAT GAC ACT GCA CAA-3'	Apoptosis

III. ***Aif*-overexpression study**

In order to confirm the concentration of AIF, as well as the relative concentrations of the AIF1 and AIF2 isoforms, we used the sense and antisense primers presented in the following table.

***Aif*-overexpressed study**			
Gene	**Sense**	**Antisense**	**Function**
Total *AIF*	5'- TAT TTC CAG CCA CCT TCT TTC-3'	5'-TTC ACC ATG TTG CCT CTT AC-3'	Apoptosis
AIF1	5'-AGT CCT TAT TGT GGG CTT ATC-3'	5'-GCA ATG GCT CTT CTC TGT T-3'	Apoptosis
AIF2	5'-TTC TTA ATT GTA GGA GCA ACA GT-3'	5'-CCC ATC ACT CTT TCA TTG TAT CT-3'	Apoptosis
Sdha	5'-TTG CCT TGC CAG GAC TTA-3'	5'-CAC CTT GAC TGT TGA TGA GAA T-3'	Reference gene

3.6 MITOCHONDRIAL DNA COPY NUMBER MEASUREMENT (I & II)

Total DNA from the cortex was isolated using a genomic DNA isolation kit (DNeasy Blood & Tissue Kit, Qiagen). The amount of mitochondrial DNA relative to nuclear genomic DNA was determined by RT-qPCR. The nuclear gene was *Ywhaz* and the mitochondrial gene was *ND4*. The relative mitochondrial DNA level was calculated based on the threshold cycle (Ct) as $2^{-\Delta}$ (ΔCt).

Chchd4 haploinsufficiency and *Aif2* KO studies			
Gene	**Sense**	**Antisense**	**Function**
Ywhaz	5'-GAG GAA GAA TCG TGA GTT AGT T-3'	5'-TGG TGA TGG TTG AGA CAG A-3'	Nuclear gene
ND4	5'-CCT CAG TTA GCC ACA TAG C-3'	5'-GAT TCG TTC GTA GTT GGA GTT-3'	Mitochondrial gene

3.7 RNA EXTRACTION AND SEQUENCING (II & III)

Cortical samples from P9 WT and *Aif2* KO mice (for study II) and from P9 WT and *Aif* overexpression mice (for study III) were prepared for RNA sequencing. Total RNA from each sample was extracted using an RNeasy Mini kit (Qiagen), and the library preparation was done using an MGI Easy mRNA Library Prep Kit (BGI, Inc., Wuhan, China.) following the manufacturer's instructions. The sequencing library was used for cluster generation and sequencing on the BGISEQ-500 system (BGI, Inc.) [117]. The sequencing was repeated 10 times, and the DESeq method was used to screen for differentially expressed genes between the two groups according to the criteria of a fold change >2 and $q < 0.01$ for study II and $p < 0.05$ for study III. The Kyoto Encyclopedia of Genes and Genomes (KEGG) pathway enrichment analysis and Gene Ontology (GO) term classification were performed using the cluster profiler R package [118].

3.8 IMMUNOBLOTTING AND ENZYME ACTIVITY ANALYSIS

3.8.1 SAMPLE PREPARATION FOR IMMUNOBLOTTING AND ENZYME ACTIVITY ANALYSIS

In order to perform immunoblotting and enzyme activity analysis, the samples required additional steps to homogenize the tissue and, in some cases, to isolate different cellular fractions (mitochondrial fraction, nuclear fraction, and cytosolic fraction) with the highest possible level of purity.

The animals used for this purpose were sacrificed by decapitation at 6–8 h or 24 h after HI. Control mice were sacrificed on P9. The pups were deeply anesthetized by intraperitoneal administration of 50 mg/ml of sodium phenobarbital and intracardially perfusion-fixed with PBS and 5% buffered formaldehyde (Histofix; Histolab Products AB, Västra Frölunda, Sweden). The brains then were rapidly dissected out on a bed of ice after the perfusion, and the parietal cortex (including the hippocampus) was dissected out from

each hemisphere and ice-cold isolation buffer was added (15 mM Tris-HCl, pH 7.6, 320 mM sucrose, 1 mM DTT, 1mM $MgCl_2$, 3 mM EDTA-K, 0.5% protease inhibitor cocktail (P8340; Sigma), added fresh immediately prior to use, and 2.5 µM cyclosporin A). For the first two studies, homogenization of the parietal cortex was performed gently by hand in a 2 ml glass/glass homogenizer (Merck Euro lab, Dorset, UK) with two different pestles with a total clearance of 0.12 mm and 0.05 mm, respectively. For the last two studies, homogenization was made by using a 2 ml Dounce tissue grinder set (D8938, Sigma, Darmstadt, Germany). In both cases, 10 gentle strokes were made using each of the pestles.

Half of the homogenates were aliquoted and stored at −80°C, and the other half were used for the fraction-isolation protocol, in which the samples were centrifuged at 800 × *g* for 10 min at 4°C. The pellets were washed in homogenizing buffer and recentrifuged at 800 × *g* for 15 min at 4°C, producing a crude nuclear pellet that was then was washed, recentrifuged, and saved as the nuclear fraction. The supernatant from the first centrifugation was further centrifuged at 9200 × *g* for 15 min at 4°C, producing a crude cytosolic fraction in the supernatant and a mitochondrial and synaptosomal fraction in the pellet, which was washed in homogenizing buffer and recentrifuged at 9,200 × g for 15 min at 4ºC. All fractions were stored at −80°C.

3.8.2 CASPASE ACTIVITY ASSAY (I, III & IV)

The protein concentrations were determined with the bicinchoninic acid protein assay method adapted for microplates. Homogenate samples were mixed with extraction buffer pH 7.3 (50 mM Tris-HCl, 100 mM NaCl, 5 mM EDTA, 1 mM EGTA, 1 mM phenylmethylsulfonylfluoride (PMSF), and 1% protease inhibitor cocktail) making a total of 100 µl (for study I the proportion was 40 µl of homogenate samples and 60 µl of extraction buffer; for study III the proportion was 25 µl of homogenate samples and 75 µl of extraction buffer). After incubation for 15 min at room temperature, 100 µl of assay buffer pH 7.3 (50 mM Tris, 100 mM NaCl, 5 mM EDTA, 1 mM EGTA, 1 mM PMSF, and 4 mm dithiothreitol (DTT) (instead of the 1% protease inhibitor cocktail added in the extraction buffer)) containing 25 µM caspase 3 substrate (#SAP3171v, Peptide Institute, Osaka, Japan) was added to each well. The cleavage of Ac-DEVD-AMC was measured for 1–2 h taking readings every 2 min at 37ºC with an excitation wavelength of 380 nm and an emission wavelength of 460 nm using a Spectramax Gemini microplate fluorometer and expressed as pmol of aminomethyl coumarin (AMC)/mg protein per minute. An endpoint reading was taken before and after adding 10 µl free AMC (100 pmol, #MCA3099-v, peptide int.) to a few of the wells.

The formula for calculating the activity was as follows:

(Vmax (linear phase) × 60 (sec to min) × 1000/µl of sample used (25 µl or 60 µl) × 100 (pmol AMC)) / (Diff AMC (reading after AMC – reading before AMC) × protein concentration).

3.8.3 OTHER ASSAYS USED IN THE STUDY

- **Glutathione reductase activity assay (study I)**

For study I, mitochondrial isolated fraction samples were used for glutathione reductase activity measurement according to the manufacturer's instructions of assay (K761-200, Biovision, Milpitas, CA, USA). Briefly, 100 µl from each sample was mixed together with 5 µl 3% H_2O_2 and incubated at 25°C for 5 min. Afterwards, 5 µl of catalase was added and the solution was mixed and incubated at 25°C for 5 min. A total volume of 25 µl of the pretreated samples was placed into a 96-well plate, and assay buffer was added to 50 µl. A total of 50 µl reaction mix was added, and the absorbance was measured immediately at 450 nm in kinetic mode for 60 min at 37°C. The activity was calculated according to the standard curve and expressed as mU/mg protein.

- **Phosphorylated and total p53 assay (study I)**

For study I, mitochondrial and cytosolic isolated fraction samples were used for investigating the levels of phosphorylated p53 (pS15) and total p53 protein in a semi-quantitative way from both controls and at 6 h after HI of WT and *chchd4*-haploinsufficient mice samples. The p53 protein assay was performed as per the manufacturer's recommendations (p53 (pS15) + Total p53 SimpleStep ELISA Kit, Abcam, ab205713, UK). Briefly, the serially diluted control and diluted sample, both 50 µl, were mixed with 25 µl capture antibody and 25 µl detector antibody and then incubated for 1 h at room temperature on a plate shaker set to 400 rpm. After three washes, 100 µl TMB (3,3',5,5'-tetramethylbenzidine) substrate was added to each well. Samples were incubated for 15 min in the dark on a plate shaker at 400 rpm, and the reactions were stopped by adding 100 µl stop solution to each well. After shaking for 1 min, the OD was recorded at 450 nm. Data were normalized by protein concentration and expressed as unit/mg protein.

- **Mitochondria isolation and respiration assay (study I)**

For study I, mitochondrial isolated fraction samples were used for investigating the mitochondrial respiration, which was measured in a high-resolution respirometer with concentration-dependent background correction (Oroboros Instruments, Innsbruck, Austria). The respiratory control ratio was calculated as the ratio of the state 3 respiration rates following the second ADP addition to the resting respiration rate (state 4) [119].

- **Oxidative stress assay (study II)**

For study II, different assays were used with the samples in order to study the effect of *Aif2* KO on the level of oxidative stress after HI. The levels of malondialdehyde (MDA) (TBARS assay kit, Cayman Chemical), protein carbonylation (Abcam, ab126287, Cambridge, UK), glutathione (GSH) (R&D System, Minneapolis, MN, USA), and catalase expression (Thermo Fisher Scientific Inc. EIACATC, Carlsbad, CA, USA) in the HI and control brains were measured with commercially available kits according to the manufacturers' instructions. The absorbance was read on a microplate reader (Molecular Devices Corp., Sunnyvale, CA, USA).

- **OxPhos complex I enzyme activity assay (study III)**

For study III, mitochondrial isolated fraction samples were used for investigating OxPhos complex I enzyme activity using a specific assay for this purpose (ab109721, Abcam, Cambridge, UK). Protein extraction was prepared by adding 1/10 volume of 10× detergent solution to 20 µl samples with equal protein concentration and then incubating on ice for 30 min. The supernatant was collected by centrifuging at 16,000 × *g* for 20 min at 4°C and then diluting the samples to the desired concentration in incubation solution. The sample (200 µl) was added to the pre-coated microplate (200 µl of incubation solution was added to measure the background signal), and the microplate was incubated for 3 hours at 21ºC. After washing with wash buffer solution, 200 µl of assay solution (1× dilution buffer, 20× NADH, and 100× dye) was added to each well. The plate was read in kinetic mode, and the OD at 450 nm was measured every 30 seconds for 30 min at 21ºC. The result was expressed as mean optical density (mOD)min/100 µg protein.

- **CypA measurement in the nuclear fraction (III & IV)**

For studies III and IV, we wanted to check the levels of CypA in the nucleus after HI because it is a good indicator that the AIF/CypA complex has translocated to the nucleus. This was especially important for study III because we wanted to show that the blocking peptide was actually working. The levels of CypA were measured by using the CypA kit abx585050 (Abbexa, Cambridge, UK) in the nuclear fraction of the samples. Following the manufacturer's instructions, the samples (which were previously centrifuged at 1000 × *g* for 20 min to remove the precipitant and the supernatants were diluted appropriately) were added to a pre-coated plate that was covered and incubated for 90 min at 37ºC. After the incubation, the liquid was discarded and 100 µl biotin-conjugated antibody was added to each well. The plate was sealed and incubated for 60 min at 37ºC. The solution was discarded and the plate was washed three times with 350 µl washing buffer. After completely removing the washing buffer, 100 µl of horseradish peroxidase solution was

added and incubated for 30 min at 37ºC. The liquid was discarded and the plate was washed five times. A total of 90 µl TMB substrate was added and incubated for 20 min at 37ºC in the dark. After the final incubation, 50 µl stop solution was added to end the reaction, and the absorbance at 450 nm was immediately analyzed on a microplate reader (Molecular Devices Corp., Sunnyvale, CA, USA). The result was expressed as µg/mg protein.

3.8.4 IMMUNOBLOTTING

Samples were thawed on ice, and the total protein concentration was determined using the bicinchoninic acid method. A total of 65 µl of each brain sample (whether it was the whole homogenized brain or a specific cellular fraction) was mixed with 25 µl NuPAGE LDS 4× sample buffer (NP0007, ThermoFisher Scientific, Carlsbad, CA, USA) and 10 µl reducing agent (NP0004, ThermoFisher Scientific, Carlsbad, CA, USA) and then heated at 70°C for 10 min. Individual samples were run on 4–12% Invitrogen NuPAGE Bis-Tris gels (Novex, San Diego, CA, USA) and, following the manufacturer's instructions, MOPS or MES SDS running buffer was used depending on the size of the proteins we wanted to investigate (MOPS for medium and high molecular weight proteins and MES for low molecular weight proteins, both from ThermoFisher Scientific, Carlsbad, CA, USA). Afterwards, the membranes were transferred to reinforced nitrocellulose membranes (Schleicher & Schuell, Dassel, Germany, for the first two studies and Bio-Rad for the last two studies). After blocking with 30 mM Tris-HCl (pH 7.5), 100 mM NaCl, and 0.1% Tween 20 containing 5% fat-free milk powder for 1 h at room temperature, the membranes were incubated with primary antibodies for 60 min at room temperature. The antibodies used for each study are listed below, together with their specific dilutions.

***Chchd4* haploinsufficiency study**				
Protein	**Animal**	**Dilution**	**Company**	**Clonality**
AIF	Goat	1:1000	sc-9416, Santa Cruz	Polyclonal
Caspase-3	Rabbit	1:1000	H-277, Santa Cruz	Polyclonal
Cy c	Mouse	1:500	clone 7H8.2C12, BD Biosciences	Monoclonal
CHCHD4	Rabbit	1:500	sc-98628, Santa Cruz	Polyclonal
Fodrin	Mouse	1:500	clone AA6, BIOMOL	Monoclonal
OxPhos Complex 1 39 kDa subunit	Mouse	1:1000	clone 20C11, Molecular Probes	Monoclonal
Total OxPhos	Mouse	1:250	MS604, MitoSciences	Monoclonal
Smac	Rabbit	1:500	sc-227766, Santa Cruz	Polyclonal
HSP70	Mouse	1:500	c-7298, Santa Cruz	Monoclonal
p53	Mouse	1:500	sc-99, Santa Cruz	Monoclonal
SOD2	Mouse	1:1000	clone 2A1, Lab Frontier	Monoclonal
Histone H3	Rabbit	1:500	06-755, Millipore	Polyclonal
Phospho-DRP1	Rabbit	1:1000	4867, Cell Signaling	Polyclonal
DRP1	Mouse	1:300	sc-271583, Santa Cruz	Monoclonal
Syn1	Goat	1:500	sc-7379, Santa Cruz	Polyclonal
OPA1	Mouse	1:1000	612606, BD Biosciences	Monoclonal
MFN1	Mouse	1: 500	NBP1-71775, Novusbio	Monoclonal
FIS1	Rabbit	1: 500	FL-152, sc-98900, Santa Cruz	Polyclonal
TIMM8A	Rabbit	1: 500	DDP1, 11179-1-AP, Proteintech	Polyclonal
Actin	Rabbit	1:200	A2066, Sigma	Polyclonal

***Aif2* KO study**				
Protein	**Animal**	**Dilution**	**Company**	**Clonality**
AIF	Goat	1:1000	sc-9416, Santa Cruz	Polyclonal
Cy c	Mouse	1:500	clone 7H8.2C12, BD Biosciences	Monoclonal
CHCHD4	Rabbit	1:500	sc-98628, Santa Cruz	Polyclonal
OxPhos Complex 1 39 kDa subunit	Mouse	1:1000	clone 20C11, Molecular Probes	Monoclonal
SOD2	Mouse	1:1000	clone 2A1, Lab Frontier	Monoclonal
HSP70	Mouse	1:500	sc-7298, Santa Cruz	Monoclonal
Actin	Rabbit	1:200	A2066, Sigma	Polyclonal

Aif-overexpression study				
Protein	**Animal**	**Dilution**	**Company**	**Clonality**
AIF	Rabbit	1:1000	E20, ab32516, Abcam	Monoclonal
ANTI-FLAG	Mouse	1:1000	M2, F1804, Sigma	Monoclonal
CHCHD4	Mouse	1:200	C-12, sc-365137, Santa Cruz	Monoclonal
COX1	Rabbit	1:1000	EPR19628, ab203912, Abcam	Monoclonal
PGC1α	Rabbit	1:1000	PA5-38021, ThermoFisher	Polyclonal
TFAM	Rabbit	1:1000	A13552, ABclonal	Polyclonal
SOD2	Rabbit	1:1000	A1340, ABclonal	Polyclonal
Cyt c	Mouse	1:500	6H2, sc-13561, Santa Cruz	Monoclonal
Phospho-DRP1	Rabbit	1:1000	Ser637, 4867, Cell Signaling	Polyclonal
OPA1	Mouse	1:1000	612606, BD Bioscience	Monoclonal
MFN1	Mouse	1: 500	NBP1-71775, Novusbio	Monoclonal
FIS1	Rabbit	1:500	FL-152, sc-98900, Santa Cruz	Polyclonal
PARP-1	Rabbit	1:1000	E102, ab32138, Abcam	Monoclonal
Cleaved PARP-1	Rabbit	1:1000	E51, ab32064, Abcam	Monoclonal
Lamin B	Goat	1:200	M-20, sc-6217, Santa Cruz	Polyclonal
VDAC1	Mouse	1:500	B-6, sc-390996, Santa Cruz	Monoclonal

Inhibition of AIF/CypA complex study				
Protein	**Animal**	**Dilution**	**Company**	**Clonality**
AIF	Rabbit	1:1000	E20, ab32516, Abcam	Monoclonal
Lamin B	Goat	1:200	M-20, sc-6217, Santa Cruz	Polyclonal

After washing the membranes three times for 5 min each, they were incubated with a peroxidase-labeled secondary antibody for 30 min at room temperature (goat anti-rabbit 1:2,000 dilution, horse anti-goat 1:2,000 dilution, or horse anti-mouse 1:4,000 dilution). Immunoreactive species were visualized using the SuperSignal West Pico PLUS Chemiluminescent Substrate (34580, ThermoFisher Scientific, Rockford, IL, USA) and a LAS 3000 cooled CCD camera (Fujifilm, Tokyo, Japan).

3.9 ELECTRON MICROSCOPY (II)

For study II, we thought it was important to show if there were any changes in the ultrastructure of the mitochondria or in the average number and size of mitochondria per brain cell in the cortex. In order to do so, we decided to prepare some samples for an electron microscopy analysis. The brain samples were perfused as previously explained and then fixed in the same solution (2.5% glutaraldehyde, 2% paraformaldehyde, 0.05% sodium azide, and 0.05 M sodium cacodylate) for 24 h and afterwards transferred to PBS. Whole

hemispheres were sliced into 0.5 mm thick coronal sections, and pieces from the parietal cortex were collected. Post-fixing was performed in 1% OsO_4 at 4°C for 2 h, and the samples were treated with 0.5% aqueous uranyl acetate for 2 h. The samples were dehydrated and embedded in epoxy resin (Agar 100 Resin). Ultrathin sections (60 nm) were cut on a Reichert Ultramicrotome (Reichert Microscope Services, Depew, NY, USA), post stained with 5% uranyl acetate, and examined with a LEO 912AB transmission electron microscope (Carl Zeiss NTS GmbH, Oberkochen, Germany) equipped with a Proscan and a Megaview III camera (Olympus Soft Imaging Solutions GmbH, Münster, Germany).

3.10 OVARY HISTOLOGY ANALYSIS (II)

The effect of *Aif2* KO on fertility required the study of the follicular development in female ovaries. For this purpose, ovaries were fixed in 4% paraformaldehyde, dehydrated, and then embedded in paraffin. The paraffin-embedded ovaries were serially sectioned at 8 mm thickness and rehydrated followed by staining with hematoxylin for morphological observation. Ovarian follicles at different developmental stages were categorized based on the well-accepted standards established by Pedersen and Peters [120].

3.11 BEHAVIORAL EVALUATION (II)

Because the HI-induced brain damage is observed in several parts of the brain, and because the effects are long lasting because the extent of the injury is too great for the regenerative processes of the brain, we wanted to determine if there were any difference in the deficits in motor and cognitive functions in adult mice after HI was performed at P9. In the *Aif2* KO study, behavioral assessments after HI were conducted using the open-field test and DigiGait analysis.

- **Open field**

The open-field test is a simple test of locomotor activity involving the observation of an animal's movements within an open arena in order to observe the exploration-related motor activity, habitation, and anxiety-related activity. When a mouse is placed in an unfamiliar field (20 cm × 20 cm square arena with 30 cm high walls made of gray polypropylene), it will typically move around the new place but stay close to the walls. After a while, the mouse will become more familiarized with the environment and will start moving around the new place from one wall to another by crossing the central portion of the arena. At this point, the number of stops and time spent in the middle of the

arena can be tracked and recorded, and also the total distance traveled during the 20-min observation period, starting by always placing the mouse in the center of the arena. The middle of the animal's body was defined as the point for tracking entries into different zones. The data were recorded using the View II software (BIOBSERVE, Germany) and automatically summarized every 5 minutes. The arena was cleaned with 70% alcohol after each animal was tested [121].

- **DigiGait analysis**

DigiGait equipment was purchased from Mouse Specifics, Inc. (Boston, USA), and this is nowadays one of the most widely published videography instrumentations available for gait analysis in mice. Briefly, each mouse was placed on a motor-driven treadmill with a transparent treadmill belt and imaged from beneath with a high-speed digital video camera. A minimum of three seconds of images are required for DigiGait analysis, and only mice that were able to run at the chosen speed for the entire process were qualified. Color images were converted to their binary matrix equivalents, and the areas of the moving paws relative to the belt and camera were calculated throughout each stride. This was used to generate a dynamic gait signal of the paw placement relative to the treadmill belt and camera. Each limb's gait signal was used to calculate the time for one complete stride for the paw under analysis (stride duration). This was broken down into subcomponents of stance duration (the time during which the paw is in contact with the treadmill) and swing duration (the time during which the paw is above the walking surface and not in contact with the belt). Stance duration further comprises the braking phase (time from initial paw contact with the treadmill to maximum paw contact) and propulsion duration (time from maximum paw contact to lifting from the treadmill). Stride width was defined as the perpendicular distance between the centroids of each set of axial paws during peak stance. Gait symmetry was measured as the ratio of forelimb stepping frequency to hind limb stepping frequency.

3.12 STATISTICS

The Statistical Package for the Social Sciences versions 21.0, 22.0, and 23.0 (SPSS, IBM, NY, USA) and GraphPad Prism Software (GraphPad Software, San Diego, CA, USA) versions 6 and 8 were used for all the analyses. Comparisons between experimental groups were performed by Student's *t*-test, assuming that samples followed a normal distribution. For multiple comparisons, one-way ANOVA (LSD and Bonferroni tests) was used when the homoscedasticity (equal variances) was assumed between groups. Data with unequal variance were compared with the Mann–Whitney *U*-test. Results

are presented as means ± standard errors of the mean, and statistical differences were considered significant when $p < 0.05$. For study III, two-way ANOVA followed by Sidak's post hoc test was used for multiple comparisons of data from more than two groups.

3.13 THE PROJECT DESIGN

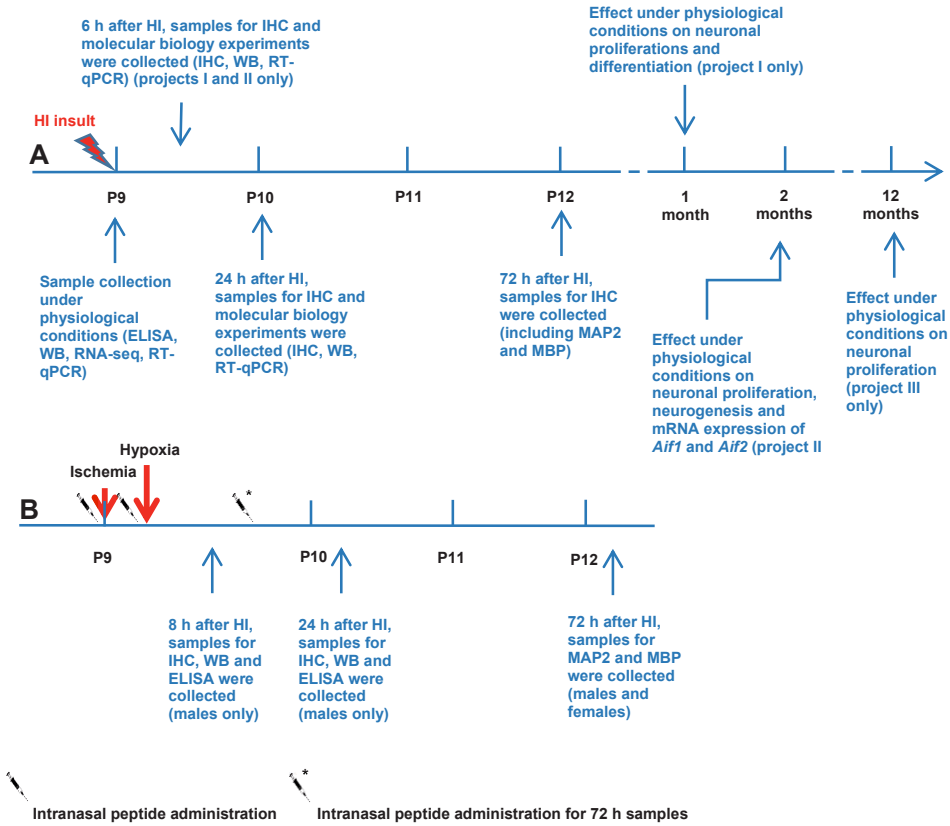

Figure 5. A. *Schematic representation of the study design for papers I, II and III, and the type of experiments performed for each time point.* ***B.*** *Schematic representation of the study design for paper IV, including the administration of the AIF(370-394)-TAT peptide and the different experiments performed for each time point.*

4 RESULTS

4.1 *CHCHD4* HAPLOINSUFFICIENCY IN A MOUSE MODEL OF HIE

Several immunoblots were performed in the cytosolic and nuclear fractions as well as in the homogenized brain tissue for both wild and heterozygous P9 mice groups. Under physiological conditions, the results showed that the total amount of CHCHD4 protein was about 25% less in the *Chchd4*-haploinsufficient brain homogenate than the WT littermates. At the same time, immunoblotting in the mitochondrial fraction showed that other relevant proapoptotic proteins (AIF, Cyt c, and Smac), superoxide dismutase 2 (SOD2), and HSP70 showed no difference between groups (also under physiological conditions). However, after HI, *Chchd4* downregulation affected the protein concentration of AIF (at 24 h post-HI), Cyt c (at 24 h post-HI), and SOD2 (at 6 h and at 24 h post-HI), having higher values of these proteins in the mitochondria after HI, indicating that *Chchd4* haploinsufficiency was preventing these proteins from leaving the mitochondria after HI.

The results in this study showed that *Chchd4* downregulation reduces neuronal cell death and caspase-independent apoptotic cell death, which affords neuroprotection by reducing the release of MIMS proteins, such as AIF (at 24h post-HI), and Cyt c (at 24 h post-HI) [122]. This phenomenon caused a reduction in the brain injury volume by 21.5% at 72 hours post-HI in $Chchd4^{+/-}$ mice, affecting all the different brain regions analyzed (cortex, hippocampus, striatum, and thalamus) as shown in the MAP2 studies. When analyzing the results separating the mice by sex, both male and female mice reached a significant difference, but the tissue loss volume was reduced by 26.6% in male *Chchd4*-haploinsufficient mice and by 15.8% in female *Chchd4*-haploinsufficient mice. We also studied the total tissue loss volume at 4 weeks after the insult, and we found that it was reduced by 31.3% in $Chchd4^{+/-}$ mice indicating that the neuroprotective effect of *Chchd4* haploinsufficiency was long lasting.

The effect of *Chchd4* reduction on cell death was corroborated by Fluoro-Jade and AIF-positive nuclear staining, showing a significant decrease of Fluoro-Jade positive cells in the cortex at 24 h post-HI in $Chchd4^{+/-}$ mice and a reduction in AIF-positive nuclei in the cortex at 6 h and at 24 h after HI. *Chchd4* downregulation also afforded long-term neuroprotection, and the brain injury volume was reduced by 31.3% at four weeks after HI.

Quantification of immunoblots of cortex homogenates showed that fodrin degradation was not significantly different between groups in the IL hemisphere for either of the two bands generated by its degradation (one 120 kDa induced by caspase 3 activation and the other 150 kDa induced by necrotic cell death caused by calpain activation). In another immunoblot focusing on the quantification of the caspase 3 cleavage band, neither showed any difference, nor did the caspase 3 activity assay performed on the homogenized IL brain tissue.

Chchd4 haploinsufficiency had no influence on mitochondrial biogenesis, as shown by mRNA expression of peroxisome proliferator-activated receptor γ coactivator-1α (*Pgc1α*) and mitochondrial transcription factor A (*Tfam*), together with mtDNA copy number assay results (both under physiological conditions and after HI). In this regard, we found no difference either when performing an immunoblotting of individual respiratory chain complex CI, CII, CIII, CIV, and CV subunits in the mitochondrial fraction of WT and CHCHD4-haploinsufficient mice under physiological conditions. Dynamic changes in mitochondria were also studied, including fusion (mitochondrial optic atrophy 1 (*Opa1*) and mitofusion (*Mfn1, Mfn2*)) and fission (dynamin-1-like protein (*Drp1*), mitochondrial fission 1 (*Fis1*), and mitochondrial fission factor (*Mff*)) genes, showing no differences in physiological conditions or during the first hours post-HI in the mRNA expression or immunoblotting between groups. No effect on cellular redox capacity was observed, as measured by RT-qPCR in Keap1-NRF2 pathway-related genes under physiological conditions or during the first hours post-HI. All of these mitochondrial data suggested that *Chchd4* haploinsufficiency did not affect mitochondrial functions including biogenesis, fusion, fission, or redox capacity.

There were also no significant changes in the expression or distribution of p53 protein (according to the immunoblotting results in cytosolic, mitochondrial, and nuclear fractions, together with homogenate brain tissue, both under physiological conditions and at 6–24 h after the insult). Nor were there any differences between groups under physiological conditions or after HI in the expression of p53 pathway-related genes (mRNA expression of *p53*, *p21*, p53-upregulated modulator of apoptosis (*PUMA*), and *Mdm2* genes).

Finally, *Chchd4* haploinsufficiency had no influence on neural stem cell proliferation or differentiation, as measured by BrdU labeling in 1-month-old mice for both groups and quantified in the granular layer of the DG, and this corroborated the BLBP labeling results in the SGZ.

4.2 EFFECT OF *AIF2* KO IN A MOUSE MODEL OF HIE

As mentioned above, *Aif1* and *Aif2* only differ in a short stretch in the N-terminal region, translated from exon 2, and that is removed from the mature protein as it translocates to the nucleus. However, the effects of knocking out *Aif2* has never been studied before under physiological conditions or after HI. Therefore, we performed a number of experiments under both physiological and pathological conditions to better understand the role of AIF2 [123].

The first step was to measure the relative abundance of *Aif1* and *Aif2* mRNA transcripts in the brains from the WT control and conditional *Aif2* KO mice littermates for neonatal (P9) and adult (P60) mice under physiological conditions. In WT mice, we found a natural increase in *Aif2* expression with age, while *Aif1* expression remained stable. However, in adult *Aif2* KO mice the relative *Aif1* mRNA level was 90% higher compared to the WT littermates. Immunoblotting in P9 mice showed no differences in the mitochondria-related proteins analyzed (CHCHD4, Cyt c, SOD2, HSP70, and Cytochrome c oxidase subunit I (COXI)), including total AIF (AIF1 and AIF2 protein concentrations).

Further investigations under physiological conditions to study the effect of *Aif2* KO in P60 mice showed that neurogenesis, as measured by DCX-labeled cells, increased by 27% when this isoform was knocked out. However, the number of Ki67-labeled cells was similar for both groups. This was the only important effect observed, and no visible phenotypic differences between *Aif2* KO and WT mice were seen in terms of survival, fertility, or neurobehavioral tests (open field and DigiGait) in adult mice and no differences were seen in follicular development in *Aif2* KO ovaries. KEGG pathway enrichment analyses did not reveal any remarkable changes in gene expression as analyzed by transcriptome sequencing between the two groups at P9. As a final set of investigations under physiological conditions, several mitochondrial properties were assessed, including mitochondrial morphology and distribution in cortical neurons (investigated by electron microscopy), mitochondrial respiratory activity (indicated by the respiratory control ratio (state 3 respiration/state 4 respiration)), mitochondrial biogenesis (by mtDNA copy number assay), mitochondrial respiratory chain complex subunit expression in the mitochondrial fraction, and mitochondrial biogenesis-related fusion-related and fission-related gene assay (by transcriptome analysis based on specific genes for the two processes). We found no differences between P9 WT and *Aif2* KO pups in any of these experiments.

We then proceeded to study the effect of HI in our *Aif2* KO mice. HI-induced gray-matter injury in P9 mice was evaluated by MAP2 immunohistochemistry staining at 72 h post-HI. The tissue loss and infarction volume were significantly greater in *Aif2* KO mice compared to WT mice, as corroborated by the total neuropathological score, and encompassed all four studied brain regions (cortex, striatum, hippocampus, and thalamus). Immunohistochemistry staining for active caspase 3-labeled cells and AIF-positive nuclei showed that the quantification of the positive cells in selected regions of the brain at 6 h and 24 h after HI were not significantly different between the groups.

Finally, we thoroughly studied the effect of *Aif2* KO on oxidative stress. *Aif2* KO induced oxidative stress, as shown by 8-OHG–positive nuclei (a marker of oxidative damage to nucleic acids) at 6 h after HI, and the proportion of positive cells was significantly higher in the cortex (61%) and striatum (53%) in *Aif2* KO mice compared to WT mice. Protein nitrosylation (measured by 3-NT staining) was also significantly higher in the cortex, striatum, and CA1 of the hippocampus in *Aif2* KO mice compared to WT mice at 6 h post-HI. Together with the previously mentioned immunohistochemistry analysis, we performed four different assays – MDA, protein carbonylation, GSH, and catalase activity – to further investigate the effect of the *Aif2* KO in the oxidative stress process, and all were performed under physiological conditions and at 6 h and 24 h after the insult. We found that while there was a general increase in the values after HI for both groups, specifically two of them (MDA values at 24 h post-HI and catalase values at 6 h post-HI) were significantly higher in the *Aif2* KO group compared to the WT littermates.

All in all, these data suggest that there is a compensatory effect in the expression level of *AIF1* when *AIF2* is knocked out and that this change in the AIF1/AIF2 protein ratio leads to increased brain injury after HI insult together with increased vulnerability to oxidative stress.

4.3 EFFECT OF *AIF* OVEREXPRESSION ON HI BRAIN INJURY

As mentioned above, since the discovery of AIF, the role of this protein in the caspase-independent apoptotic process has been studied through several diverse approaches. However, the effect of overexpressing AIF on neonatal cerebral HI has not been studied. By using an *Aif*-overexpressed transgenic mouse, we investigated the effect of the protein from this perspective.

Our results showed that in this mouse the mRNA expression of the *Aif1* isoform was 5.9 times higher at P9 than in WT control mice under physiological conditions (taking into consideration both endogenous and exogenous *Aif*). However, the expression of *Aif2* was not affected in our transgenic mice. The mRNA transcriptome under physiological conditions showed no relevant differentially expressed genes between groups in the cortex.

At the protein level, where our western blot methods are unable to distinguish between the two versions of AIF, the results showed that the total amount of AIF protein was 2.4 times higher in the transgenic overexpression mice compared to WT littermates. At this protein level, we did not find any differences in other mitochondria-related proteins (including CHCHD4, COXI, Cyt c, or SOD2), in mitochondrial biogenesis-related proteins (PGC1α and TFAM), or in fission and fusion-related proteins (P-DRP1, FIS1, OPA1, and MFN1). The activity of mitochondrial OxPhos complex I was measured and showed no differences in oxidative phosphorylation in neonatal *Aif*-overexpression mice compared to WT mice. Furthermore, our transgenic mouse did not show any phenotypic differences in terms of body weight or mortality when they were 1 year old, but, as suggested by the results from DCX-positive cell analysis in the SGZ of the DG, there was a significant increase in neurogenesis in *Aif*-overexpression mice compared to WT mice.

This showed the effect of *Aif*-overexpression under physiological conditions, but we were particularly interested in how these transgenic mice respond to HI. Our hypothesis was that increased expression of *Aif* (particularly *Aif1*) could potentially increase the pro-apoptotic activity of AIF. Indeed, *Aif* overexpression significantly increased the severity of brain injury after HI. MAP2 staining at 72 h after HI showed that the infarction volume was increased by 74.6%, and this was corroborated by the total neuropathological scored. *Aif* overexpression increased HI-induced brain injury in all observed brain regions, particularly in the cortex, hippocampus, and striatum, as well as in the NH region. MBP staining at 72 h after HI showed that the total lost volume of subcortical white matter in the IL hemisphere was greater in the *Aif* overexpressing mice compared to WT littermates.

AIF nuclear translocation was significantly increased at 24 h post-HI in all the brain regions studied (including the cortex, CA1, striatum, and NH) as shown by AIF-positive nuclear immunostaining. By using an immunofluorescence staining which could differentiate between endogenous and exogenous AIF, we confirmed that exogenous AIF contributes to HI-induced nuclear translocation and apoptotic cell death. We also measured the effect of *Aif*

overexpression on the caspase-dependent apoptotic pathway at 24 h post-HI, and while caspase 3-positive cells were significantly increased in the cortex and striatum, no changes were seen in the CA1 or NH regions. In order to further investigate this pathway, a caspase 3 activity assay was performed in the parietal cortex (including the hippocampus), and this showed no differences in the IL samples between groups. Similarly, a PARP1 assay showed no differences in cleavage in the IL cortex between the two groups.

We have also shown that more AIF protein was released from the mitochondria after HI in the *Aif* overexpression mice by quantification of immunoblotting in the mitochondrial fraction at 24 h after HI, and specifically exogenous AIF was reduced in the mitochondria by 18%. Quantification of mitochondria-related proteins (including CHCHD4, COXI, Cyt c, and SOD2) did not show any significant differences between IL brain samples from WT and *Aif* overexpression mice, apart from an increase in CHCHD4 protein levels in the IL hemisphere compared to the CL hemisphere in both groups. As before, we are not able to distinguish between isoforms (AIF1 and AIF2), so we relied on RT-qPCR to measure the mRNA expression of *Aif1* and *Aif2*. *Aif1* mRNA expression was significantly upregulated in both WT and AIF overexpression mice compared to their controls, while *Aif2* was significantly downregulated in both WT and AIF overexpression mice.

We also measured the protein concentration of CypA in the nuclear fraction, and a significant increase was observed in the IL hemispheres compared to the CL hemispheres for both groups. Focusing on the IL hemisphere, there was a significant increase of CypA in the *Aif* overexpression mice compared to their WT littermates, corroborating that CypA translocated to the nucleus after HI and that this translocation was increased when *Aif* was overexpressed. Finally, we studied the expression of fission and fusion-related proteins (P-DRP1, FIS1, OPA1, and MFN1) at 24 h post-HI, and while the results showed that mitochondrial fusion was compromised after HI, there was no difference between WT and *Aif* overexpression mice with respect to the cleavage of OPA1 and the depletion of MFN1.

Taken together, this study showed that excessive AIF (specifically the AIF1 isoform) does not cause obvious phenotypic changes or alterations in the physiological functions, but does aggravate HI-induced injury in the neonatal mouse brain, correlating with an increase in the translocation of AIF to the nucleus of brain cells.

4.4 INHIBITION OF THE AIF/CYPA COMPLEX

The effect of the AIF(370-394)-TAT peptide treatment on brain injury in neonatal mice was evaluated by dividing the experiments into two groups.

First, we evaluated the brain injury at 72 h after HI by analyzing the immunohistochemistry results based on MAP2 and MBP staining for gray and white matter respectively, as previously explained. We collected all the mice for each group (half treated with the AIF(370-394)-TAT peptide and the other half treated with vehicle and used as controls) from both sexes. The infarction volumes in AIF(370-394)-TAT–treated mice were significantly reduced by 48.1% compared to vehicle-treated littermates. The average infarction volume was 63.3% smaller in treated male mice, while for females the average values showed a tendency to decrease but without reaching statistical significance. The neuropathological score in the different brain regions analyzed (cortex, hippocampus, striatum, and thalamus) showed that in AIF(370-394)-TAT–treated mice there was only a significant difference in the striatum (reduced by 24.6%, $p < 0.05$), while there was only a non-significant tendency for a decrease in the cortex, hippocampus, and thalamus. Again, this difference was more pronounced in male mice, with a reduction in the injury severity by about 50% in the striatum and thalamus, and no differences were observed in female mice in any of the specific brain regions examined. The ratio of the MBP-positive subcortical white matter in the IL hemisphere to that of the CL hemisphere showed a significant increase of 21.7% in peptide-treated mice compared to vehicle-treated mice, meaning that the subcortical white matter was less injured in AIF(370-394)-TAT–treated mice at 72 h post-HI. Once more, the proportion in males was even higher (25.0%) in peptide-treated male mice compared to vehicle-treated mice, whereas in females the difference was much milder and was not statistically significant.

Second, another group of mice was selected for investigating the effect of the peptide at 8 h and at 24 h after HI. For this purpose, we decided to focus on male mice only based on the brain injury evaluation at 72 h after HI. It was an important point to prove that the peptide was actually blocking the translocation of AIF to the nucleus and to determine if it was also affecting the translocation of CypA into brain cells after HI. The best way to confirm this was to extract the nuclear fraction from homogenized brain tissue (cortex + hippocampus) from both groups and then perform the experiments to determine if there was any difference in the amount of AIF and CypA present in the nuclei of brain cells at 8 h and 24 h after HI. The protein expression of AIF in neonatal male mice by immunoblotting in the nuclear fraction extracted from the total brain homogenate showed that at 8 h post-HI the values were

similar for both groups. However, at 24 h after the insult the AIF accumulation in the nuclear fraction was 3.6 times higher in the vehicle-treated group, while in the AIF(370-394)-TAT–treated male mice the concentration of translocated AIF showed only a mild increase, giving a significant difference between groups and meaning that AIF(370-394)-TAT treatment prevented AIF accumulation in the nucleus at 24 h post-HI. We corroborated this finding by measuring CypA expression in the nuclear fraction in neonatal male mice by immunoblotting, and again we found that at 8 h post-HI there was no significant difference between peptide-treated and vehicle-treated mice, but at 24 h post-HI the amount of CypA protein translocated to the nucleus was much greater in the control group, while in peptide-treated mice the effect was ameliorated. The final confirmation came from a CypA assay in the nuclear fraction, showing lower CypA at 8 h post-HI in treated male mice compared to control littermates, and the reduction in CypA became even greater at 24 h after HI, with a 55% reduction in AIF(370-394)-TAT–treated mice compared to vehicle-treated mice.

Neuronal cell death in different brain regions (cortex, striatum, the CA1 sector of the hippocampus, and the NH) was investigated using Fluoro-Jade labeling, a non-specific neuronal cell death marker, and there was a general decrease in Fluoro-Jade–positive cells in AIF(370-394)-TAT–treated mice in the IL hemisphere compared to the IL hemisphere of vehicle-treated mice. The difference was statistically significant in the CA1 region at 8 h post-HI and in the NH region at 24 h post-HI. We then investigated caspase-dependent apoptotic cell death as indicated by active caspase-3 immunohistochemical labeling in brain sections. We found no significant differences between the two groups at any of the time points. The numbers of AIF-positive nuclei counted in AIF(370-394)-TAT–treated male mice decreased significantly in the cortex, striatum, and NH at 8 h after HI compared to vehicle-treated male mice; however, at 24 h post-HI, the numbers of AIF-positive nuclei tended to equilibrate.

In summary, the administration of the synthetic AIF370-394 peptide with the cell-penetrating TAT peptide inhibited *in-vivo* formation of the AIF/CypA complex and its translocation to the nucleus, and thereby reduced brain injury after HI in neonatal mice.

5 DISCUSSION

5.1 ROLE OF CHCHD4 IN A MOUSE MODEL OF HIE

After HI, several forms of cell death occur in the neonatal brain, including apoptosis (caspase-dependent and caspase-independent pathways), necrosis, autophagy, and several hybrid phenotypes between them, and together these are referred to as the cell death continuum [124]. Several factors are critical for the different forms of cell death, and although the mechanisms driving the cell death continuum are partly unknown, the severity of the insult, sex, and age seem to be major factors [125].

It has been established that AIF's pro-survival function requires a functional CHCHD4 protein, and *Aif* depletion is correlated with decreased CHCHD4 protein level (without affecting mRNA transcription) [100]. In the *Chchd4*-happloinsufficiency study, we have shown that reducing the protein expression of the *Chchd4* gene by 25% reduced brain damage in P9 mice after HI but did not affect AIF protein expression, suggesting that CHCHD4 acts by blocking the AIF release from the mitochondria upon apoptotic stimuli (as well as blocking Cyt c release). mRNA and protein expression of SOD2 (an important protein that protects against superoxide radicals and is located in the mitochondrial matrix) is reduced after HI [126], and *Chchd4* depletion also prevented this HI-induced SOD2 reduction. While AIF-positive nuclei results showed that AIF was prevented from being translocated to the nucleus, fodrin degradation and caspase 3-like activity (DEVDase) showed no significant difference between groups, and therefore the protective role of CHCHD4 in the brain is most likely through the caspase-independent apoptotic pathway.

Mitochondrial biogenesis, as well as mitochondrial fusion/fission activity, showed no differences between WT and *Chchd4*$^{+/-}$ mice under either physiological or pathological conditions, hence the neuroprotection observed in the *Chchd4*$^{+/-}$ mice cannot be explained by these biological processes.

Among its multiple biological functions, p53 has been reported to translocate to the mitochondria in the early stages of reperfusion after HI in neonatal rats mediated by CHCHD4, and this might be involved in the mitochondrial membrane pore opening [127]. Decreased CHCHD4 expression showed a reduced accumulation of p53 in the mitochondria while increasing its nuclear activity [128]. However, in this study we did not find any significant changes in p53 expression or cellular distribution of p53 under either physiological or

pathological conditions, and we did not even see increased accumulation of p53 in the mitochondria after HI, suggesting that the role of p53 in cell death might be different depending on the species, age, or type of insult.

Overall, these results suggest that *Chchd4* downregulation provides neuroprotection by preventing the translocation of AIF to the nucleus and by ameliorating the reduction in SOD2 usually observed in the mitochondria after HI.

5.2 ROLE OF AIF2 IN A MOUSE MODEL OF HIE

AIF has been shown to be a major contributor to caspase-independent neuronal loss induced by neonatal cerebral HI, and the Hq mice, which have an 80% reduction in the expression of the protein (including both isoforms AIF1 and AIF2), showed an impressive reduction of brain injury after HI (52.6% and 41% reduction in infarct volume at 72 h post-HI for males and females, respectively) [83]. However, the brain-specific isoform AIF2 has barely been studied. Therefore, we investigated the specific role of AIF2 in brain damage. Previously, one of the few studies on AIF2 showed that in humans the mRNA expression of *AIF2* was higher in adult brain than in fetal brain, while the mRNA expression of *AIF1* was lower [85]. As explained before, the AIF2 isoform is only expressed in the brain, but Hangen and colleagues showed that its distribution is not homogeneous. For example, approximately 25% of the cells present in the anterior olfactory nucleus stained uniquely for the exon 2b-specific probe, indicating the existence of brain cells that express AIF2, but not AIF1. In that paper it was also mentioned that AIF2 is more difficult to dissociate from the mitochondrial membrane than AIF1 due to the changes in the AA sequences that affect the region of the protein that is anchored in the IMM, hypothesizing that AIF2 might contribute less efficiently to apoptosis than AIF1 [85]. AIF has the ability to form dimers or higher-order oligomers, and these complexes can potentially be formed by both AIF1 and/or AIF2 isoforms. Upon apoptosis stimuli, the heterodimers or hetero-oligomers containing one or more AIF2 isoforms would be less likely to be released into the cytosol. Therefore, we speculated that the AIF1/AIF2 ratio in the IMM might be crucial for the pro-apoptotic role of AIF.

The results in our *Aif2* KO study showed that by eliminating the expression of AIF2, AIF1 will increase its expression under physiological conditions by 38% in P9 mice and by 90% in P60 mice as a compensatory reaction. This increase, together with the fact that the AIF2 isoform is not expressed, increases the AIF1/AIF2 ratio substantially.

AIF is essential for embryonic development, and without it the programmed cell death necessary during cavitation of embryoid bodies does not occur [69]. While *Aif* KO mice are embryonically lethal, Hq mice are viable but display severe phenotypes [71]. However, in this study we found that AIF2 is not essential for mouse viability, and no phenotype was observed in *Aif2* KO adult mice under physiological conditions in terms of fertility, mortality, or neurobehavioral tests. In fact, P9 mice showed no alteration in the expression of proteins such as Cyt c, SOD2, HSP70, or COXl. CHCHD4 physically interacts with AIF, and the protein expression of both of them is linked because experiments with embryonic mice showed that *Aif* depletion or downregulation caused a depletion of CHCHD4 protein, while high expression of CHCHD4 rescued the problems associated with low levels of AIF, and low levels of CHCHD4 led to the same problems as low levels of AIF [100; 105]. However, here we found that CHCHD4 protein expression was not affected by *Aif2* KO in P9 mice.

The only effect observed in *Aif2* KO mice under physiological conditions was an increase in neurogenesis as measured by DCX-labeled cells, which was increased by 27% in the SGZ of the DG of the hippocampus in P60 mice. The number of Ki67-labeled cells, however, was not significant. Ki67 is a proliferation marker, and DCX appears after differentiation of new neurons, thus labeling immature neurons at a time when NeuN is not yet expressed. Interestingly, Hq mice showed progressive loss of adult cerebellar and retinal neurons, and in experiments with *Aif* KO embryos, the mutant mice had midbrain defects and dramatic deficits in cerebellar Purkinje and granule cell precursors [70].

AIF is a free radical scavenger, and Hq mice, which have reduced AIF levels, have increased concentrations of hydroperoxides in their brains and thus experience increased oxidative stress [71; 83]. *Aif2* KO mice have higher levels of markers of oxidative stress, including 8-OHG, 3-NT, and MDA, without significant changes in GSH levels or the Keap1-Nrf2 pathway. This suggests that local redox equilibria are affected by the changes in the AIF1/AIF2 ratio, caused either by the lack of AIF2 or the overabundance of AIF1. However, the role of the AIF2 isoform in redox reactions is still unknown.

Aif2 KO mice showed greater severity of brain damage as measured by the infarction area at 72 h after HI. However, immunohistochemistry showed no differences in caspase 3-positive cells or AIF-positive nuclei. Because the translocation to the nuclei was similar in *Aif2* KO compared to WT mice, the most plausible explanation for the increase in the injury severity would be the increased oxidative stress in the KO mice, which might be caused by the

difference in the AIF1/AIF2 ratio. Although requiring further study, our results suggest that AIF2 is a better free radical scavenger than AIF1 and that AIF1 and AIF2 differ in their roles in the neonatal brain after HI.

5.3 Effect of *Aif*-OVEREXPRESSION IN A MOUSE MODEL OF HIE

In this study, instead of studying the effect of *Aif2* KO, we focused on the effect of overexpressing *Aif1* in P9 mice (5.9 times higher than WT under physiological conditions) without affecting *Aif2* expression. This translated to a 2.4-fold increase in the expression of total AIF protein.

Similar to the *Aif2* KO study, the phenotype was totally normal, with the exception of an increase in neurogenesis (as suggested by the results from DCX-positive cell analysis in the SGZ of the DG). For both cases (*Aif2* KO and *Aif* overexpression), AIF1 seems to be involved in neurogenesis but not AIF2.

Under pathological conditions, the mice had increased severity of brain injury. In this case, the immunohistochemistry results showed that AIF-positive nuclei were higher in the overexpression mice, affecting all the brain regions analyzed, and both exogenous and endogenous AIF participated in the translocation. Caspase 3-positive cells also showed increased numbers in the *Aif* overexpression mice compared to WT, but this occurred only in the cortex and striatum. This finding might be explained by the different compositions of neuronal subpopulations and densities, and it is possible that there might be different cell death pathways in the different brain regions. Overall these results showed that the caspase-independent pathway was more affected by the *Aif* overexpression than the caspase-dependent cell death.

After HI, the reduction of AIF protein in the mitochondrial fraction was greater in the *Aif* overexpression mice (affecting both endogenous and exogenous AIF protein), but the rest of the mitochondrial-related proteins showed no differences compared to WT mice. Interestingly, RT-qPCR with homogenized cortical tissue from both groups at 24 h post-HI showed that while *Aif1* mRNA expression was significantly upregulated in both WT and *Aif* overexpression mice, *Aif2* mRNA expression was significantly downregulated in both groups after HI.

As explained above, AIF needs to cooperate with CypA in order to be able to translocate to the nucleus and perform, together with H2AX, chromatinolysis

and large-scale DNA degradation. The protein levels of CypA were higher in the nuclear fraction of the overexpression mice after HI, indicating that the AIF/CypA complex was involved in the increase in AIF translocation upon HI.

HI insult induced caspase 3 activation and PARP-1 cleavage at 24 h, but no significant differences were found between the two groups, suggesting that the preferences in the cell death pathway might differ between brain regions, sex, age, or severity or type of pathological condition.

Overall, increased expression of AIF1, while not generating phenotypic changes, except for an increase in neurogenesis, amplified the brain damage in neonatal mice by increasing the translocation of AIF to the nucleus and brain-specific caspase 3 activation, indicating the important role of the caspase-independent protein AIF in neonatal HI brain injury.

5.4 PHARMACOLOGICAL INHIBITION OF THE AIF/CYPA COMPLEX *IN VIVO*

Since the discovery that CypA participates in the nuclear translocation of AIF [78], it has been suggested to be a target for inhibiting AIF translocation after HI. Before that, some studies showed alternatives for that aim, like targeting the antiapoptotic BCL-2 family proteins [129] or preventing the translocation of AIF to the nucleus by overexpressing HSP70 [130]. Cyclophilins influence the conformation of proteins in cells, among other functions [131]. CypA is an abundant, ubiquitously expressed protein, and it is particularly highly expressed in neurons [132]. In healthy neurons, CypA is localized both in the cytoplasm and nuclei, and it is not essential for mammalian cell viability, as indicated by the fact that *CypA* KO embryonic stem cells grow normally and differentiate into hematopoietic precursor cells *in vitro* [133]. In 2007, Zhu and colleagues showed that in a *CypA* KO study in mice, the total infarct volume was reduced by 46.7%, and the total tissue loss was reduced by 33.8% compared to the WT littermates after HI without affecting the mitochondrial release of cell death effectors [78].

The AIF(370-394)-TAT peptide was shown *in vitro* to block the AIF/CypA complex in the cytosol prior its translocation to the nucleus by competing with AIF for binding to CypA and it showed neuroprotective effects in a model of glutamate-induced oxidative stress in cultured HT-22 cells (an immortalized mouse hippocampal cell line subcloned from the HT-4 cell line that is highly sensitive to glutamate and is thus frequently used as a model system to study glutamate-induced toxicity in neuronal cells [134]) while preserving their

mitochondrial integrity [135]. The peptide inhibited AIF from reaching the nucleus in this study to a similar extent as *CypA*-siRNA [135]. The data here showed that the peptide also works *in vivo* in mice and that it has neuroprotective effects. The infarction volume was significantly lower in the peptide-treated mice compared to vehicle-treated littermates ($p = 0.0084$), as indicated by the MAP2 staining. The detailed analysis of the infarction volume by sex showed a significant decrease in males ($p = 0.0021$) but not in females. Furthermore, the pathological score showed that the striatum was less damaged in peptide-treated mice. Here again we found a sex difference, where males showed a better response to the treatment, especially in the striatum and thalamus regions, than females. MBP staining revealed consistent results with grey-matter analysis, and the ratio of MBP-positive areas in the IL and CL hemispheres showed significantly higher values in peptide-treated mice compared to vehicle-treated mice ($p = 0.018$), meaning that the reduction of white matter was lower when using the AIF(370-394)-TAT peptide. Similarly, as with the MAP-2 staining results, the effect was more pronounced in males than in females.

Sex differences in perinatal brain injury have previously been reported. PARP-1 is a nuclear enzyme involved in DNA repair, but it is also involved in a unique PARP-1–dependent cell death program when the DNA damage is severe [98], and this process is closely linked to AIF when apoptosis is triggered by acute neurological insult [57]. Some years ago, in a PARP-1 study, Hagberg and colleagues found that *Parp1* KO provided significant protection in mice of both sexes [99]. Similarly with our study presented here, analysis by sex in that study revealed that males were strongly protected, while females were not. The degree of PAR accumulation during the first hours (1–4 h) after HI was similar in female and male P7 mice, but there was a drop in NAD+ in males, and not in females. There are other studies reporting sex differences when using TH after HI, resulting in more effective long-term protection in female than in male 7-day-old rats [102]. Furthermore, based on the analysis of the cell death mechanisms, it has been shown that, at least in neuron cell culture, the caspase-independent pathway is more predominant in males and, in contrast, the caspase-dependent pathway is more prevalent in females [100; 101]. Also, while there was no sex difference in brain injury at any age when the HI insult was severe, when the insult was moderate, adult (60 days old) male mice displayed more severe injury compared to females [101]. In this paper we have shown again that the AIF apoptotic pathway seems to be more prevalent in males than in females because at 72 h after the insult the blocking peptide provided greater protection in males. For the 8–24 h studies we only used male mice and thus the early response in females is still unclear at this stage.

There is some controversy regarding how the interaction between AIF and CypA enables their translocation into the nucleus [136]. One model suggests the independent translocation of both proteins prior to chromatinolysis and DNA fragmentation, and this is supported by the results in a necrosis model in which CypA down-regulation did not compromise the nuclear translocation of AIF but did reduce the extent of DNA damage [79]. The other model proposes that upon apoptotic stimuli, AIF and CypA form a complex in the cytosol, and this interaction allows both proteins to translocate to the nucleus and induce cell death. The results we have presented here, in which the nuclear translocation of AIF after HI was significantly reduced in *CypA* KO mice compared to WT littermates, would seem to support the hypothesis that CypA plays a fundamental role in the translocation of AIF into the nucleus, at least in this male mouse phenotype after HI [78]. Here we show that the AIF(370-394)-TAT peptide reduced the protein levels of AIF in the nuclear fraction at 24 h after HI, and at the same time we showed that the levels of CypA in the cytosol were decreased at 8 h and 24 h after HI, again in accordance with the second model, in the sense that the CypA and AIF proteins might cooperate and translocate together into the nucleus, without discarding the hypothesis in which CypA is able to translocate into the nucleus independent of AIF in the earliest stages after HI [135].

Caspase 3 activation is a hallmark of caspase-dependent apoptotic cell death, and our results showed that even though the caspase 3 values were similar at 8 h after HI between peptide-treated and control mice, there was a drastic reduction in caspase 3 activity at 24 h after the insult. The reason behind this phenomenon suggest crosstalk between AIF and caspase 3, which would explain the severe reduction in caspase 3 activity without affecting the number of caspase 3-positive cells. Further analysis regarding this intriguing matter will help better our understanding of the connections between the different cell death pathways.

6 FINAL CONCLUSIONS

The final conclusions of this work are summarized in the following key points:

CHCHD4 and AIF are **crucial proteins** for brain damage after HI insult in young mice.

Chchd4 haploinsufficiency leads to persistent neuroprotection related to **reduced release of MIMS proteins** such as AIF and Cyt c.

An increase in the expression level of AIF1 when *Aif2* is knocked out induces a change in the **AIF1/AIF2 ratio** that promotes increased oxidative stress and subsequent brain injury after HI. In the same way, overexpressing AIF1 also led to increased brain damage in neonatal mice after HI.

Under physiological conditions, increased expression of AIF1, either by knocking out *Aif2* or by knocking in a proviral insertion of *Aif1*, promoted neurogenesis in adult mice, with no other phenotypic changes.

The mechanisms in which brain cells carry out the different apoptotic pathways are likely to show **sex differences**, and our peptide that inhibited the formation of AIF/CypA complex showed a greater neuroprotective effect in male mice compared to female mice.

ACKNOWLEDGEMENT

It has been an exciting journey, full of experiences and learnings throughout the four years of my PhD. Here I would like to acknowledge those who have contributed the most for this book to happen, whether for scientific or personal reasons. Without the help of people who have supported me during this project I wouldn't have achieved much.

First of all, I would like to express my deepest gratitude to my main supervisor **Changlian Zhu**, not only for accepting me as a PhD student in your lab and providing me opportunities to work with you, but also for your support, mentoring, inspiration and for sharing your knowledge. I'm very happy to have been part of your group. Your guidance, patience, positiveness and advices have been an invaluable source of encouragement. Thank you for being always there whenever I have needed your help.

Second, I would like to thank my co-supervisors: **Carina Mallard** and **Henrik Hagberg**, for fruitful discussions and important advices on my research and for your support during my time here. Your help and kindness were inestimable.

Thank you to all the past and current members of our main lab group: **Yanyan Sun**, **Kai Zhou**, **Cuicui Xie**, **Yafeng Wang**, **Kenan Li, Yong Wang, Shan Zhang** and **Yiran Xu**. You all warmly welcomed me since the first day I arrived to the lab and you made me feel very conformable and as if I was part of the group since the very beginning, and you were always willing to help me regardless how busy you were, even though the help required to stay in the lab till very late. And special thanks to **Tao Li**, the person with who I have spent most of the time in the lab and in the office, discussing a lot of experiments and results. You helped me a lot at the beginning, teaching me a lot of new techniques and optimizing them to get the best possible results, and also in how to use new software and to interpret the results. The time spent discussing about our results were one of the most productive parts of my PhD, and it was a pleasure to do it.

I also want to thank to all the colleagues on the S-floor: **Lars Karlsson**, **Malin Johansson**, **Reza Motalleb**, **Parthenia Savvidi**, **Eva Brigos**, **Dilip Kumar Malipatlolla**, **Piyush Patel**, **Oona Lagström**, **Klara Danielsson**, **Mia Ericson**, **Rita Grandér**, **Georg Kuhn**, **Mats Sandberg**, **Cecilia Bull** and all the others who work or have worked on the S-floor or on any of the other floors of the building, making this a cheerful place to work and, of course, to fika.

I also acknowledge the **Centre for Cellular Imaging** (CCI), for expertise in imaging and technical assistance. The photo included in the front cover of this thesis was taken at the CCI facility.

Thank you to all my friends here, specially to **Gravina Gravina** (also known as Giacomo Gravina) for all those breaks having coffees and talking about past, present and future. **Davide Lovera** and **Pasquale Cocchiaro,** for making the first part of my PhD much funnier in between experiments, to **Axel Andersson** for the funny talks (and for the help with the Swedish translation of the abstract), and to all the rest of my friends working in Sahlgrenska or from outside the academia. The dilution 1:3 has now a huge impact factor.

And finally, I would like to thank to all my friends all over the world and to my family. Thank you all for your support.

REFERENCES

[1] F. Gonzalez, and S. Miller, Does perinatal asphyxia impair cognitive function without cerebral palsy? Archives of Disease in Childhood-Fetal and Neonatal Edition 91 (2006) F454-F459.

[2] M. Van Handel, H. Swaab, L.S. De Vries, and M.J. Jongmans, Long-term cognitive and behavioral consequences of neonatal encephalopathy following perinatal asphyxia: a review. European journal of pediatrics 166 (2007) 645-654.

[3] N. Marlow, A. Rose, C. Rands, and E. Draper, Neuropsychological and educational problems at school age associated with neonatal encephalopathy. Archives of Disease in Childhood-Fetal and Neonatal Edition 90 (2005) F380-F387.

[4] N. Badawi, J.J. Kurinczuk, J.M. Keogh, L.M. Alessandri, F. O'Sullivan, P.R. Burton, P.J. Pemberton, and F.J. Stanley, Antepartum risk factors for newborn encephalopathy: the Western Australian case-control study. Bmj 317 (1998) 1549-1553.

[5] J.J. Kurinczuk, M. White-Koning, and N. Badawi, Epidemiology of neonatal encephalopathy and hypoxic–ischaemic encephalopathy. Early human development 86 (2010) 329-338.

[6] M. Douglas-Escobar, and M.D. Weiss, Hypoxic-ischemic encephalopathy: a review for the clinician. JAMA Pediatr 169 (2015) 397-403.

[7] M. Hayakawa, Y. Ito, S. Saito, N. Mitsuda, S. Hosono, H. Yoda, K. Cho, K. Otsuki, S. Ibara, and K. Terui, Incidence and prediction of outcome in hypoxic–ischemic encephalopathy in J apan. Pediatrics International 56 (2014) 215-221.

[8] A. García-Alix, M. Martínez-Biarge, J. Diez, F. Gayá, and J. Quero, Neonatal hypoxic-ischemic encephalopathy: Incidence and prevalence in the first decade of the 21st century, Anales de pediatria (Barcelona, Spain: 2003), 2009, pp. 319-326.

[9] K.R. Gopagondanahalli, J. Li, M.C. Fahey, R.W. Hunt, G. Jenkin, S.L. Miller, and A. Malhotra, Preterm Hypoxic–ischemic encephalopathy. Frontiers in pediatrics 4 (2016) 114.

[10] B. Larroque, P.-Y. Ancel, S. Marret, L. Marchand, M. André, C. Arnaud, V. Pierrat, J.-C. Rozé, J. Messer, and G. Thiriez, Neurodevelopmental disabilities and special care of 5-year-old children born before 33 weeks of gestation (the EPIPAGE study): a longitudinal cohort study. The Lancet 371 (2008) 813-820.

[11] R. Galinsky, C.A. Lear, J.M. Dean, G. Wassink, S.K. Dhillon, M. Fraser, J.O. Davidson, L. Bennet, and A.J. Gunn, Complex interactions between hypoxia-ischemia and inflammation in preterm brain injury. Developmental Medicine & Child Neurology 60 (2018) 126-133.

[12] L. Bennet, L. Van Den Heuij, J. M Dean, P. Drury, G. Wassink, and A. Jan Gunn, Neural plasticity and the K ennard principle: does it work for the preterm brain? Clinical and Experimental Pharmacology and Physiology 40 (2013) 774-784.

[13] H.B. Sarnat, and M.S. Sarnat, Neonatal encephalopathy following fetal distress: a clinical and electroencephalographic study. Archives of neurology 33 (1976) 696-705.

[14] G.D. Hankins, and M. Speer, Defining the pathogenesis and pathophysiology of neonatal encephalopathy and cerebral palsy. Obstetrics & Gynecology 102 (2003) 628-636.

[15] K. Lindström, P. Lagerroos, C. Gillberg, and E. Fernell, Teenage outcome after being born at term with moderate neonatal encephalopathy. Pediatric neurology 35 (2006) 268-274.

[16] M. Bracken, and J. Sinclair, Effective care of the newborn infant, Oxford: Oxford University Press, 1992.

[17] A.D. Edwards, P. Brocklehurst, A.J. Gunn, H. Halliday, E. Juszczak, M. Levene, B. Strohm, M. Thoresen, A. Whitelaw, and D. Azzopardi, Neurological outcomes at 18 months of age after moderate hypothermia for perinatal hypoxic ischaemic encephalopathy: synthesis and meta-analysis of trial data. Bmj 340 (2010) c363.

[18] G. Carli, I. Reiger, and N. Evans, One-year neurodevelopmental outcome after moderate newborn hypoxic ischaemic encephalopathy. Journal of paediatrics and child health 40 (2004) 217-220.

[19] M.A. Tagin, C.G. Woolcott, M.J. Vincer, R.K. Whyte, and D.A. Stinson, Hypothermia for neonatal hypoxic ischemic encephalopathy: an updated systematic review and meta-analysis. Archives of pediatrics & adolescent medicine 166 (2012) 558-566.

[20] R.D. Higgins, T. Raju, A.D. Edwards, D.V. Azzopardi, C.L. Bose, R.H. Clark, D.M. Ferriero, R. Guillet, A.J. Gunn, and H. Hagberg, Hypothermia and other treatment options for neonatal encephalopathy: an executive summary of the Eunice Kennedy Shriver NICHD workshop. The Journal of pediatrics 159 (2011) 851-858. e1.

[21] A.J. Gunn, and T.R. Gunn, Thepharmacology'of neuronal rescue with cerebral hypothermia. Early human development 53 (1998) 19-35.

[22] K. Fairchild, D. Sokora, J. Scott, and S. Zanelli, Therapeutic hypothermia on neonatal transport: 4-year experience in a single NICU. Journal of Perinatology 30 (2010) 324.

[23] P.P. Drury, L. Bennet, and A.J. Gunn, Mechanisms of hypothermic neuroprotection, Seminars in Fetal and Neonatal Medicine, Elsevier, 2010, pp. 287-292.

[24] O. Iwata, S. Iwata, J.S. Thornton, E. De Vita, A. Bainbridge, L. Herbert, F. Scaravilli, D. Peebles, J.S. Wyatt, and E.B. Cady, "Therapeutic time window" duration decreases with increasing severity of cerebral hypoxia–ischaemia under normothermia and delayed hypothermia in newborn piglets. Brain research 1154 (2007) 173-180.

[25] D. Adstamongkonkul, and D.C. Hess, Ischemic conditioning and neonatal hypoxic ischemic encephalopathy: a literature review. Conditioning medicine 1 (2017) 9.

[26] C.M. Traudt, R.J. McPherson, L.A. Bauer, T.L. Richards, T.M. Burbacher, R.M. McAdams, and S.E. Juul, Concurrent erythropoietin and hypothermia treatment improve outcomes in a term nonhuman primate model of perinatal asphyxia. Dev Neurosci 35 (2013) 491-503.

[27] R.D. Barrett, L. Bennet, J. Davidson, J.M. Dean, S. George, B.S. Emerald, and A.J. Gunn, Destruction and reconstruction: hypoxia and the developing brain. Birth Defects Research Part C: Embryo Today: Reviews 81 (2007) 163-176.

[28] D.V. Azzopardi, B. Strohm, A.D. Edwards, L. Dyet, H.L. Halliday, E. Juszczak, O. Kapellou, M. Levene, N. Marlow, and E. Porter, Moderate hypothermia to treat perinatal asphyxial encephalopathy. New England Journal of Medicine 361 (2009) 1349-1358.

[29] S.E. Juul, Hypothermia plus erythropoietin for neonatal neuroprotection? Commentary on Fan et al. and Fang et al. Pediatric research 73 (2013) 10.

[30] C. Zhu, W. Kang, F. Xu, X. Cheng, Z. Zhang, L. Jia, L. Ji, X. Guo, H. Xiong, G. Simbruner, K. Blomgren, and X. Wang, Erythropoietin improved neurologic outcomes in newborns with hypoxic-ischemic encephalopathy. Pediatrics 124 (2009) e218-26.

[31] L. Wang, Z. Zhang, Y. Wang, R. Zhang, and M. Chopp, Treatment of stroke with erythropoietin enhances neurogenesis and angiogenesis and improves neurological function in rats. Stroke 35 (2004) 1732-1737.

[32] P. Villa, P. Bigini, T. Mennini, D. Agnello, T. Laragione, A. Cagnotto, B. Viviani, M. Marinovich, A. Cerami, and T.R. Coleman, Erythropoietin selectively attenuates cytokine production and

inflammation in cerebral ischemia by targeting neuronal apoptosis. Journal of Experimental Medicine 198 (2003) 971-975.
[33] B. Dixon, C. Reis, W. Ho, J. Tang, and J. Zhang, Neuroprotective strategies after neonatal hypoxic ischemic encephalopathy. International journal of molecular sciences 16 (2015) 22368-22401.
[34] D. Alonso-Alconada, A. Álvarez, O. Arteaga, A. Martínez-Ibargüen, and E. Hilario, Neuroprotective effect of melatonin: a novel therapy against perinatal hypoxia-ischemia. International journal of molecular sciences 14 (2013) 9379-9395.
[35] A.-K. Welin, P. Svedin, R. Lapatto, B. Sultan, H. Hagberg, P. Gressens, I. Kjellmer, and C. Mallard, Melatonin reduces inflammation and cell death in white matter in the mid-gestation fetal sheep following umbilical cord occlusion. Pediatric research 61 (2007) 153.
[36] M.R. Cilio, and D.M. Ferriero, Synergistic neuroprotective therapies with hypothermia, Seminars in Fetal and Neonatal Medicine, Elsevier, 2010, pp. 293-298.
[37] E.P. Yıldız, B. Ekici, and B. Tatlı, Neonatal hypoxic ischemic encephalopathy: an update on disease pathogenesis and treatment. Expert Review of Neurotherapeutics 17 (2017) 449-459.
[38] C. Thornton, B. Leaw, C. Mallard, S. Nair, M. Jinnai, and H. Hagberg, Cell death in the developing brain after hypoxia-ischemia. Frontiers in cellular neuroscience 11 (2017) 248.
[39] S.J. Vannucci, and H. Hagberg, Hypoxia–ischemia in the immature brain. Journal of Experimental Biology 207 (2004) 3149-3154.
[40] J. Wyatt, A. Edwards, D. Azzopardi, and E. Reynolds, Magnetic resonance and near infrared spectroscopy for investigation of perinatal hypoxic-ischaemic brain injury. Archives of disease in childhood 64 (1989) 953-963.
[41] L. Galluzzi, K. Blomgren, and G. Kroemer, Mitochondrial membrane permeabilization in neuronal injury. Nature Reviews Neuroscience 10 (2009) 481.
[42] F.J. Northington, D.M. Ferriero, E.M. Graham, R.J. Traystman, and L.J. Martin, Early neurodegeneration after hypoxia-ischemia in neonatal rat is necrosis while delayed neuronal death is apoptosis. Neurobiology of disease 8 (2001) 207-219.
[43] K. Blomgren, and H. Hagberg, Free radicals, mitochondria, and hypoxia–ischemia in the developing brain. Free radical biology and medicine 40 (2006) 388-397.
[44] H. Hagberg, Hypoxic-ischemic damage in the neonatal brain: excitatory amino acids. Developmental pharmacology and therapeutics 18 (1992) 139-144.
[45] C.I. Rousset, A.A. Baburamani, C. Thornton, and H. Hagberg, Mitochondria and perinatal brain injury. The journal of maternal-fetal & neonatal medicine 25 (2012) 35-38.
[46] H. Hagberg, C. Mallard, C.I. Rousset, and C. Thornton, Mitochondria: hub of injury responses in the developing brain. The Lancet Neurology 13 (2014) 217-232.
[47] H. Wajant, The Fas signaling pathway: more than a paradigm. Science 296 (2002) 1635-1636.
[48] A. Shamas-Din, H. Brahmbhatt, B. Leber, and D.W. Andrews, BH3-only proteins: Orchestrators of apoptosis. Biochimica et Biophysica Acta (BBA)-Molecular Cell Research 1813 (2011) 508-520.
[49] P. Li, D. Nijhawan, I. Budihardjo, S.M. Srinivasula, M. Ahmad, E.S. Alnemri, and X. Wang, Cytochrome c and dATP-dependent formation of Apaf-1/caspase-9 complex initiates an apoptotic protease cascade. Cell 91 (1997) 479-489.
[50] R.U. Jänicke, M.L. Sprengart, M.R. Wati, and A.G. Porter, Caspase-3 is required for DNA fragmentation and morphological changes associated with apoptosis. Journal of Biological Chemistry 273 (1998) 9357-9360.

[51] D.R. Green, and F. Llambi, Cell death signaling. Cold Spring Harbor perspectives in biology 7 (2015) a006080.
[52] B.M. Polster, G. Basañez, A. Etxebarria, J.M. Hardwick, and D.G. Nicholls, Calpain I induces cleavage and release of apoptosis-inducing factor from isolated mitochondria. Journal of Biological Chemistry 280 (2005) 6447-6454.
[53] G. Cao, J. Xing, X. Xiao, A.K. Liou, Y. Gao, X.-M. Yin, R.S. Clark, S.H. Graham, and J. Chen, Critical role of calpain I in mitochondrial release of apoptosis-inducing factor in ischemic neuronal injury. Journal of Neuroscience 27 (2007) 9278-9293.
[54] L. Ravagnan, S. Gurbuxani, S.A. Susin, C. Maisse, E. Daugas, N. Zamzami, T. Mak, M. Jäättelä, J.M. Penninger, and C. Garrido, Heat-shock protein 70 antagonizes apoptosis-inducing factor. Nature cell biology 3 (2001) 839.
[55] M.B. Gill, and J.R. Perez-Polo, Hypoxia ischemia-mediated cell death in neonatal rat brain. Neurochemical research 33 (2008) 2379-2389.
[56] K.K. David, S.A. Andrabi, T.M. Dawson, and V.L. Dawson, Parthanatos, a messenger of death. Frontiers in bioscience (Landmark edition) 14 (2009) 1116.
[57] S.-W. Yu, H. Wang, M.F. Poitras, C. Coombs, W.J. Bowers, H.J. Federoff, G.G. Poirier, T.M. Dawson, and V.L. Dawson, Mediation of poly (ADP-ribose) polymerase-1-dependent cell death by apoptosis-inducing factor. Science 297 (2002) 259-263.
[58] H. Hagberg, C. Mallard, C.I. Rousset, and X. Wang, Apoptotic mechanisms in the immature brain: involvement of mitochondria. Journal of child neurology 24 (2009) 1141-1146.
[59] C. Zhu, X. Wang, F. Xu, B. Bahr, M. Shibata, Y. Uchiyama, H. Hagberg, and K. Blomgren, The influence of age on apoptotic and other mechanisms of cell death after cerebral hypoxia–ischemia. Cell death and differentiation 12 (2005) 162.
[60] C. Candé, I. Cohen, E. Daugas, L. Ravagnan, N. Larochette, N. Zamzami, and G. Kroemer, Apoptosis-inducing factor (AIF): a novel caspase-independent death effector released from mitochondria. Biochimie 84 (2002) 215-222.
[61] H.K. Lorenzo, S.A. Susin, J. Penninger, and G. Kroemer, Apoptosis inducing factor (AIF): a phylogenetically old, caspase-independent effector of cell death. Cell death and differentiation 6 (1999) 516.
[62] A.G. Porter, and A.G. Urbano, Does apoptosis-inducing factor (AIF) have both life and death functions in cells? Bioessays 28 (2006) 834-843.
[63] S.A. Susin, N. Zamzami, M. Castedo, T. Hirsch, P. Marchetti, A. Macho, E. Daugas, M. Geuskens, and G. Kroemer, Bcl-2 inhibits the mitochondrial release of an apoptogenic protease. Journal of Experimental Medicine 184 (1996) 1331-1341.
[64] N. Zamzami, S.A. Susin, P. Marchetti, T. Hirsch, I. Gómez-Monterrey, M. Castedo, and G. Kroemer, Mitochondrial control of nuclear apoptosis. Journal of Experimental Medicine 183 (1996) 1533-1544.
[65] H. Otera, S. Ohsakaya, Z.I. Nagaura, N. Ishihara, and K. Mihara, Export of mitochondrial AIF in response to proapoptotic stimuli depends on processing at the intermembrane space. The EMBO journal 24 (2005) 1375-1386.
[66] M.M. Elguindy, and E. Nakamaru-Ogiso, Apoptosis-inducing factor (AIF) and its family member protein, AMID, are rotenone-sensitive NADH: ubiquinone oxidoreductases (NDH-2). Journal of Biological Chemistry 290 (2015) 20815-20826.

[67] S.A. Susin, H.K. Lorenzo, N. Zamzami, I. Marzo, B.E. Snow, G.M. Brothers, J. Mangion, E. Jacotot, P. Costantini, and M. Loeffler, Molecular characterization of mitochondrial apoptosis-inducing factor. Nature 397 (1999) 441.
[68] N. Vahsen, C. Candé, J.J. Brière, P. Bénit, N. Joza, N. Larochette, P.G. Mastroberardino, M.O. Pequignot, N. Casares, and V. Lazar, AIF deficiency compromises oxidative phosphorylation. The EMBO journal 23 (2004) 4679-4689.
[69] N. Joza, S.A. Susin, E. Daugas, W.L. Stanford, S.K. Cho, C.Y. Li, T. Sasaki, A.J. Elia, H.-Y.M. Cheng, and L. Ravagnan, Essential role of the mitochondrial apoptosis-inducing factor in programmed cell death. Nature 410 (2001) 549.
[70] R. Ishimura, G.R. Martin, and S.L. Ackerman, Loss of apoptosis-inducing factor results in cell-type-specific neurogenesis defects. Journal of Neuroscience 28 (2008) 4938-4948.
[71] J.A. Klein, C.M. Longo-Guess, M.P. Rossmann, K.L. Seburn, R.E. Hurd, W.N. Frankel, R.T. Bronson, and S.L. Ackerman, The harlequin mouse mutation downregulates apoptosis-inducing factor. Nature 419 (2002) 367.
[72] R. Fato, C. Bergamini, S. Leoni, P. Strocchi, and G. Lenaz, Generation of reactive oxygen species by mitochondrial complex I: implications in neurodegeneration. Neurochemical research 33 (2008) 2487-2501.
[73] E. Hangen, K. Blomgren, P. Bénit, G. Kroemer, and N. Modjtahedi, Life with or without AIF. Trends in biochemical sciences 35 (2010) 278-287.
[74] G. Kroemer, L. Galluzzi, and C. Brenner, Mitochondrial membrane permeabilization in cell death. Physiological reviews 87 (2007) 99-163.
[75] C. Zhu, L. Qiu, X. Wang, U. Hallin, C. Candé, G. Kroemer, H. Hagberg, and K. Blomgren, Involvement of apoptosis-inducing factor in neuronal death after hypoxia-ischemia in the neonatal rat brain. Journal of neurochemistry 86 (2003) 306-317.
[76] S.A. Susin, H.K. Lorenzo, N. Zamzami, I. Marzo, C. Brenner, N. Larochette, M.-C. Prévost, P.M. Alzari, and G. Kroemer, Mitochondrial release of caspase-2 and-9 during the apoptotic process. Journal of Experimental Medicine 189 (1999) 381-394.
[77] V. Yuste, R. Moubarak, C. Delettre, M. Bras, P. Sancho, N. Robert, J. d'Alayer, and S. Susin, Cysteine protease inhibition prevents mitochondrial apoptosis-inducing factor (AIF) release. Cell death and differentiation 12 (2005) 1445.
[78] C. Zhu, X. Wang, J. Deinum, Z. Huang, J. Gao, N. Modjtahedi, M.R. Neagu, M. Nilsson, P.S. Eriksson, and H. Hagberg, Cyclophilin A participates in the nuclear translocation of apoptosis-inducing factor in neurons after cerebral hypoxia-ischemia. Journal of Experimental Medicine 204 (2007) 1741-1748.
[79] C. Artus, H. Boujrad, A. Bouharrour, M.N. Brunelle, S. Hoos, V.J. Yuste, P. Lenormand, J.C. Rousselle, A. Namane, and P. England, AIF promotes chromatinolysis and caspase-independent programmed necrosis by interacting with histone H2AX. The EMBO journal 29 (2010) 1585-1599.
[80] T.T. Paull, E.P. Rogakou, V. Yamazaki, C.U. Kirchgessner, M. Gellert, and W.M. Bonner, A critical role for histone H2AX in recruitment of repair factors to nuclear foci after DNA damage. Current Biology 10 (2000) 886-895.
[81] C. Cande, N. Vahsen, I. Kouranti, E. Schmitt, E. Daugas, C. Spahr, J. Luban, R.T. Kroemer, F. Giordanetto, and C. Garrido, AIF and cyclophilin A cooperate in apoptosis-associated chromatinolysis. Oncogene 23 (2004) 1514.

[82] L. Qiu, C. Zhu, X. Wang, F. Xu, P.S. Eriksson, M. Nilsson, C.M. Cooper-Kuhn, H.G. Kuhn, and K. Blomgren, Less neurogenesis and inflammation in the immature than in the juvenile brain after cerebral hypoxia-ischemia. Journal of Cerebral Blood Flow & Metabolism 27 (2007) 785-794.

[83] C. Zhu, X. Wang, Z. Huang, L. Qiu, F. Xu, N. Vahsen, M. Nilsson, P. Eriksson, H. Hagberg, and C. Culmsee, Apoptosis-inducing factor is a major contributor to neuronal loss induced by neonatal cerebral hypoxia-ischemia. Cell death and differentiation 14 (2007) 775.

[84] M. Loeffler, E. DAUGAS, S.A. SUSIN, N. ZAMZAMI, D. MÉTIVIER, A.-L. NIEMINEN, G. BROTHERS, J.M. PENNINGER, and G. KROEMER, Dominant cell death induction by extramitochondrially targeted apoptosis-inducing factor. The FASEB Journal 15 (2001) 758-767.

[85] E. Hangen, D. De Zio, M. Bordi, C. Zhu, P. Dessen, F. Caffin, S. Lachkar, J.-L. Perfettini, V. Lazar, and J. Benard, A brain-specific isoform of mitochondrial apoptosis-inducing factor: AIF2. Cell death and differentiation 17 (2010) 1155.

[86] C. Delettre, V.J. Yuste, R.S. Moubarak, M. Bras, J.-C. Lesbordes-Brion, S. Petres, J. Bellalou, and S.A. Susin, AIFsh, a novel apoptosis-inducing factor (AIF) pro-apoptotic isoform with potential pathological relevance in human cancer. Journal of Biological Chemistry 281 (2006) 6413-6427.

[87] C. Delettre, V.J. Yuste, R.S. Moubarak, M. Bras, N. Robert, and S.A. Susin, Identification and characterization of AIFsh2, a mitochondrial apoptosis-inducing factor (AIF) isoform with NADH oxidase activity. Journal of Biological Chemistry 281 (2006) 18507-18518.

[88] R. Bågenholm, U.A. Nilsson, and I. Kjellmer, Formation of free radicals in hypoxic ischemic brain damage in the neonatal rat, assessed by an endogenous spin trap and lipid peroxidation. Brain research 773 (1997) 132-138.

[89] D.M. Ferriero, Oxidant mechanisms in neonatal hypoxia-ischemia. Developmental neuroscience 23 (2001) 198-202.

[90] P.H. Chan, Reactive oxygen radicals in signaling and damage in the ischemic brain. Journal of Cerebral Blood Flow & Metabolism 21 (2001) 2-14.

[91] D.M. Ferriero, Neonatal brain injury. New England Journal of Medicine 351 (2004) 1985-1995.

[92] M.J. Lafemina, R.A. Sheldon, and D.M. Ferriero, Acute hypoxia-ischemia results in hydrogen peroxide accumulation in neonatal but not adult mouse brain. Pediatric research 59 (2006) 680.

[93] P. Schönfeld, and G. Reiser, Why does brain metabolism not favor burning of fatty acids to provide energy?-Reflections on disadvantages of the use of free fatty acids as fuel for brain. Journal of Cerebral Blood Flow & Metabolism 33 (2013) 1493-1499.

[94] M.D. Miramar, P. Costantini, L. Ravagnan, L.M. Saraiva, D. Haouzi, G. Brothers, J.M. Penninger, M.L. Peleato, G. Kroemer, and S.A. Susin, NADH oxidase activity of mitochondrial apoptosis-inducing factor. Journal of Biological Chemistry 276 (2001) 16391-16398.

[95] I.Y. Churbanova, and I.F. Sevrioukova, Redox-dependent changes in molecular properties of mitochondrial apoptosis-inducing factor. Journal of Biological Chemistry 283 (2008) 5622-5631.

[96] I.F. Sevrioukova, Redox-linked conformational dynamics in apoptosis-inducing factor. Journal of molecular biology 390 (2009) 924-938.

[97] I.F. Sevrioukova, Apoptosis-inducing factor: structure, function, and redox regulation. Antioxidants & redox signaling 14 (2011) 2545-2579.

[98] S.J. Hong, T.M. Dawson, and V.L. Dawson, Nuclear and mitochondrial conversations in cell death: PARP-1 and AIF signaling. Trends Pharmacol Sci 25 (2004) 259-64.
[99] H. Hagberg, M.A. Wilson, H. Matsushita, C. Zhu, M. Lange, M. Gustavsson, M.F. Poitras, T.M. Dawson, V.L. Dawson, F. Northington, and M.V. Johnston, PARP-1 gene disruption in mice preferentially protects males from perinatal brain injury. J Neurochem 90 (2004) 1068-75.
[100] E. Hangen, O. Féraud, S. Lachkar, H. Mou, N. Doti, G.M. Fimia, N.-v. Lam, C. Zhu, I. Godin, and K. Muller, Interaction between AIF and CHCHD4 regulates respiratory chain biogenesis. Molecular cell 58 (2015) 1001-1014.
[101] C. Zhu, F. Xu, X. Wang, M. Shibata, Y. Uchiyama, K. Blomgren, and H. Hagberg, Different apoptotic mechanisms are activated in male and female brains after neonatal hypoxia–ischaemia. Journal of neurochemistry 96 (2006) 1016-1027.
[102] E. Bona, H. Hagberg, E.M. Løberg, R. Bågenholm, and M. Thoresen, Protective effects of moderate hypothermia after neonatal hypoxia-ischemia: short-and long-term outcome. Pediatric research 43 (1998) 738.
[103] S. Weis, A. Toniazzo, B. Ander, X. Zhan, M. Careaga, P. Ashwood, A. Wyse, C. Netto, and F.R. Sharp, Autophagy in the brain of neonates following hypoxia–ischemia shows sex-and region-specific effects. Neuroscience 256 (2014) 201-209.
[104] C. Charriaut-Marlangue, V. Besson, and O. Baud, Sexually dimorphic outcomes after neonatal stroke and hypoxia-ischemia. International journal of molecular sciences 19 (2018) 61.
[105] K. Meyer, S. Buettner, D. Ghezzi, M. Zeviani, D. Bano, and P. Nicotera, Loss of apoptosis-inducing factor critically affects MIA40 function. Cell death & disease 6 (2015) e1814.
[106] H. Brooks, B. Lebleu, and E. Vivès, Tat peptide-mediated cellular delivery: back to basics. Advanced drug delivery reviews 57 (2005) 559-577.
[107] E. Vives, P. Brodin, and B. Lebleu, A truncated HIV-1 Tat protein basic domain rapidly translocates through the plasma membrane and accumulates in the cell nucleus. Journal of Biological Chemistry 272 (1997) 16010-16017.
[108] N. Doti, C. Reuther, P. Scognamiglio, A. Dolga, N. Plesnila, M. Ruvo, and C. Culmsee, Inhibition of the AIF/CypA complex protects against intrinsic death pathways induced by oxidative stress. Cell death & disease 5 (2014) e993.
[109] R.A. Sheldon, C. Sedik, and D.M. Ferriero, Strain-related brain injury in neonatal mice subjected to hypoxia–ischemia. Brain research 810 (1998) 114-122.
[110] Y. Lallemand, V. Luria, R. Haffner-Krausz, and P. Lonai, Maternally expressed PGK-Cre transgene as a tool for early and uniform activation of the Cre site-specific recombinase. Transgenic Res 7 (1998) 105-12.
[111] J.E. Rice, R.C. Vannucci, and J.B. Brierley, The influence of immaturity on hypoxic-ischemic brain damage in the rat. Annals of Neurology: Official Journal of the American Neurological Association and the Child Neurology Society 9 (1981) 131-141.
[112] H. Chen, M. Burris, A. Fajilan, F. Spagnoli, J.H. Zhang, and J. Tang, Prolonged exposure to isoflurane ameliorates infarction severity in the rat pup model of neonatal hypoxia-ischemia. Translational stroke research 2 (2011) 382-390.
[113] J. Towfighi, C. Housman, R.C. Vannucci, and D.F. Heitjan, Effect of unilateral perinatal hypoxic-ischemic brain damage on the gross development of opposite cerebral hemisphere. Neonatology 65 (1994) 108-118.

[114] C. Xie, V. Ginet, Y. Sun, M. Koike, K. Zhou, T. Li, H. Li, Q. Li, X. Wang, Y. Uchiyama, A.C. Truttmann, G. Kroemer, J. Puyal, K. Blomgren, and C. Zhu, Neuroprotection by selective neuronal deletion of Atg7 in neonatal brain injury. Autophagy 12 (2016) 410-23.

[115] K.J. Livak, and T.D. Schmittgen, Analysis of relative gene expression data using real-time quantitative PCR and the 2− ΔΔCT method. methods 25 (2001) 402-408.

[116] J. Vandesompele, K. De Preter, F. Pattyn, B. Poppe, N. Van Roy, A. De Paepe, and F. Speleman, Accurate normalization of real-time quantitative RT-PCR data by geometric averaging of multiple internal control genes. Genome biology 3 (2002) research0034. 1.

[117] Y. Xu, Y. Sun, K. Zhou, T. Li, C. Xie, Y. Zhang, J. Rodriguez, Y. Wu, M. Hu, L.R. Shao, X. Wang, and C. Zhu, Cranial Irradiation Induces Hypothalamic Injury and Late-Onset Metabolic Disturbances in Juvenile Female Rats. Dev Neurosci 40 (2018) 120-133.

[118] G.C. Yu, L.G. Wang, Y.Y. Han, and Q.Y. He, clusterProfiler: an R Package for Comparing Biological Themes Among Gene Clusters. Omics 16 (2012) 284-287.

[119] X. Wang, A.L. Leverin, W. Han, C. Zhu, B.R. Johansson, E. Jacotot, V.S. Ten, N.R. Sims, and H. Hagberg, Isolation of brain mitochondria from neonatal mice. Journal of neurochemistry 119 (2011) 1253-61.

[120] T. Pedersen, and H. Peters, Proposal for a classification of oocytes and follicles in the mouse ovary. Reproduction 17 (1968) 555-557.

[121] C. Xie, K. Zhou, X. Wang, K. Blomgren, and C. Zhu, Therapeutic benefits of delayed lithium administration in the neonatal rat after cerebral hypoxia-ischemia. PLoS One 9 (2014) e107192.

[122] Y. Sun, T. Li, C. Xie, Y. Xu, K. Zhou, J. Rodriguez, W. Han, X. Wang, G. Kroemer, N. Modjtahedi, K. Blomgren, and C. Zhu, Haploinsufficiency in the mitochondrial protein CHCHD4 reduces brain injury in a mouse model of neonatal hypoxia-ischemia. Cell Death Dis 8 (2017) e2781.

[123] J. Rodriguez, Y. Zhang, T. Li, C. Xie, Y. Sun, Y. Xu, K. Zhou, K. Huo, Y. Wang, X. Wang, D. Andersson, A. Stahlberg, Q. Xing, C. Mallard, H. Hagberg, N. Modjtahedi, G. Kroemer, K. Blomgren, and C. Zhu, Lack of the brain-specific isoform of apoptosis-inducing factor aggravates cerebral damage in a model of neonatal hypoxia-ischemia. Cell Death Dis 10 (2018) 3.

[124] C. Portera-Cailliau, D.L. Price, and L.J. Martin, Excitotoxic neuronal death in the immature brain is an apoptosis-necrosis morphological continuum. Journal of Comparative Neurology 378 (1997) 10-87.

[125] F.J. Northington, R. Chavez-Valdez, and L.J. Martin, Neuronal cell death in neonatal hypoxia-ischemia. Annals of neurology 69 (2011) 743-758.

[126] J.E. Jung, G.S. Kim, P. Narasimhan, Y.S. Song, and P.H. Chan, Regulation of Mn-superoxide dismutase activity and neuroprotection by STAT3 in mice after cerebral ischemia. Journal of Neuroscience 29 (2009) 7003-7014.

[127] C.H. Nijboer, C.J. Heijnen, M.A. van der Kooij, J. Zijlstra, C.T. van Velthoven, C. Culmsee, F. van Bel, H. Hagberg, and A. Kavelaars, Targeting the p53 pathway to protect the neonatal ischemic brain. Annals of neurology 70 (2011) 255-264.

[128] J. Zhuang, P.-y. Wang, X. Huang, X. Chen, J.-G. Kang, and P.M. Hwang, Mitochondrial disulfide relay mediates translocation of p53 and partitions its subcellular activity. Proceedings of the National Academy of Sciences 110 (2013) 17356-17361.

[129] W. Yin, G. Cao, M.J. Johnnides, A.P. Signore, Y. Luo, R.W. Hickey, and J. Chen, TAT-mediated delivery of Bcl-xL protein is neuroprotective against neonatal hypoxic–ischemic brain injury via inhibition of caspases and AIF. Neurobiology of disease 21 (2006) 358-371.
[130] Y. Matsumori, S.M. Hong, K. Aoyama, Y. Fan, T. Kayama, R.A. Sheldon, Z.S. Vexler, D.M. Ferriero, P.R. Weinstein, and J. Liu, Hsp70 overexpression sequesters AIF and reduces neonatal hypoxic/ischemic brain injury. Journal of Cerebral Blood Flow & Metabolism 25 (2005) 899-910.
[131] S. Kumari, S. Roy, P. Singh, S. Singla-Pareek, and A. Pareek, Cyclophilins: proteins in search of function. Plant signaling & behavior 8 (2013) e22734.
[132] F.M. Göldner, and J.W. Patrick, Neuronal localization of the cyclophilin A protein in the adult rat brain. Journal of Comparative Neurology 372 (1996) 283-293.
[133] J. Colgan, M. Asmal, and J. Luban, Isolation, characterization and targeted disruption of mouse ppia: cyclophilin A is not essential for mammalian cell viability. Genomics 68 (2000) 167-178.
[134] S. Tan, M. Wood, and P. Maher, Oxidative stress induces a form of programmed cell death with characteristics of both apoptosis and necrosis in neuronal cells. Journal of neurochemistry 71 (1998) 95-105.
[135] N. Doti, C. Reuther, P.L. Scognamiglio, A.M. Dolga, N. Plesnila, M. Ruvo, and C. Culmsee, Inhibition of the AIF/CypA complex protects against intrinsic death pathways induced by oxidative stress. Cell Death Dis 5 (2014) e993.
[136] N. Doti, and M. Ruvo, Relevance and therapeutic potential of CypA targeting to block apoptosis inducing factor-mediated neuronal cell death. Neural regeneration research 12 (2017) 1428.